

The Image Biomarker Standardization Initiative: standardized quantitative radiomics for highthroughput image-based phenotyping

Zwanenburg, A.; Vallières, M.; Abdalah, M. A.; Aerts, H. J. W. L.; Andrearczyk, V.; Apte, A.; Ashrafinia, S.; Bakas, S.; Beukinga, R. J.; Boellaard, R.; Bogowicz, M.; Boldrini, L.; Buvat, I.; Cook, G. J. R.; Davatzikos, C.; Depeursinge, A.; Desseroit, M.-C.; Dinapoli, N.; Viet Dinh, C.; Echegaray, S.; El Naqa, I.; Fedorov, A. Y.; Gatta, R.; Gillies, R. J.; Goh, V.; Guckenberger, M.; Götz, M.; Min Ha, S.; Hatt, M.; Isensee, F.; Lambin, P.; Leger, S.; Leijenaar, R. T. H.; Lenkowicz, J.; Lippert, F.; Losnegård, A.; Maier-Hein, K. H.; Morin, O.; Müller, H.; Napel, S.; Nioche, C.; Orlhac, F.; Pati, S.; Pfaehler, E. A. G.; Rahmim, A.; Rao, A. U. K.; Scherer, J.; Musib Siddique, M.; Sijtsema, N. M.; Socarras Fernandez, J.; Spezi, E.; Steenbakkers, R. J. H. M.; Tanadini-Lang, S.; Thorwarth, D.; Troost, E. G. C.; Upadhaya, T.; Valentini, V.; V. Van Dijk, L.; van Griethuysen, J.; van Velden, F. H. P.; Whybra, P.; Richter, C.; Löck, S.;

Originally published:

May 2020

Radiology 295(2020)2, 328-338

DOI: <https://doi.org/10.1148/radiol.2020191145>

Perma-Link to Publication Repository of HZDR:

<https://www.hzdr.de/publications/Publ-30321>

Release of the secondary publication
on the basis of the German Copyright Law § 38 Section 4.

Title

The Image Biomarker Standardization Initiative: standardized quantitative radiomics for high-throughput image-based phenotyping

Authors

Alex Zwanenburg*, Martin Vallières*, Mahmoud A. Abdalah, Hugo J.W.L. Aerts, Vincent Andrearczyk, Aditya Apte, Saeed Ashrafinia, Spyridon Bakas, Roelof J. Beukinga, Ronald Boellaard, Marta Bogowicz, Luca Boldrini, Irène Buvat, Gary J.R. Cook, Christos Davatzikos, Adrien Depeursinge, Marie-Charlotte Desseroit, Nicola Dinapoli, Cuong Viet Dinh, Sebastian Echegaray, Issam El Naqa, Andriy Y. Fedorov, Roberto Gatta, Robert J. Gillies, Vicky Goh, Matthias Guckenberger, Michael Götz, Sung Min Ha, Mathieu Hatt, Fabian Isensee, Philippe Lambin, Stefan Leger, Ralph T.H. Leijenaar, Jacopo Lenkowicz, Fiona Lippert, Are Losnegård, Klaus H. Maier-Hein, Olivier Morin, Henning Müller, Sandy Napel, Christophe Nioche, Fanny Orlhac, Sarthak Pati, Elisabeth A.G. Pfaehler, Arman Rahmim, Arvind U.K. Rao, Jonas Scherer, Muhammad Musib Siddique, Nanna M. Sijtsema, Jairo Socarras Fernandez, Emiliano Spezi, Roel J.H.M Steenbakkens, Stephanie Tanadini-Lang, Daniela Thorwarth, Esther G.C. Troost, Taman Upadhaya, Vincenzo Valentini, Lisanne V. van Dijk, Joost van Griethuysen, Floris H.P. van Velden, Philip Whybra, Christian Richter, Steffen Löck

* These authors share first authorship

Other authors are ordered alphabetically

Author affiliations

From OncoRay – National Center for Radiation Research in Oncology, Faculty of Medicine and University Hospital Carl Gustav Carus, Technische Universität Dresden, Helmholtz-Zentrum

Dresden - Rossendorf, Dresden, Germany (A.Z., S.Le, E.G.C.T., C.R., S.Lö), National Center for Tumor Diseases (NCT), Partner Site Dresden, Germany; German Cancer Research Center (DKFZ), Heidelberg, Germany; Faculty of Medicine and University Hospital Carl Gustav Carus, Technische Universität Dresden, Dresden, Germany, and; Helmholtz Association / Helmholtz-Zentrum Dresden - Rossendorf (HZDR), Dresden, Germany (A.Z., S.Le, E.G.C.T.), German Cancer Consortium (DKTK), Partner Site Dresden, and German Cancer Research Center (DKFZ), Heidelberg, Germany (A.Z., S.Le, E.G.C.T., C.R., S.Lö), Medical Physics Unit, McGill University, Montréal, Québec, Canada (M.V., I.E.N.), Image Response Assessment Team Core Facility, Moffitt Cancer Center, Tampa (FL), USA (M.A.A.), Dana-Farber Cancer Institute, Brigham and Women's Hospital, and Harvard Medical School, Harvard University, Boston (MA), USA (H.J.W.L.A.), Institute of Information Systems, University of Applied Sciences Western Switzerland (HES-SO), Sierre, Switzerland (V.A., A.D., H.M.), Department of Medical Physics, Memorial Sloan Kettering Cancer Center, New York (NY), USA (A.A.), Department of Electrical and Computer Engineering, Johns Hopkins University, Baltimore (MD), USA (S.A.), Department of Radiology and Radiological Science, Johns Hopkins University, Baltimore (MD), USA (S.A., A.R.), Center for Biomedical image Computing and Analytics (CBICA), University of Pennsylvania, Philadelphia (PA), USA (S.B., C.D., S.M.H., S.P.), Department of Radiology, Perelman School of Medicine, University of Pennsylvania, Philadelphia (PA), USA (S.B., C.D., S.M.H., S.P.), Department of Pathology and Laboratory Medicine, Perelman School of Medicine, University of Pennsylvania, Philadelphia (PA), USA (S.B.), Department of Nuclear Medicine and Molecular Imaging, University of Groningen, University Medical Center Groningen (UMCG), Groningen, The Netherlands (R.J.B., R.B., E.A.G.P.), Radiology and Nuclear Medicine, VU University Medical Centre (VUMC), Amsterdam, The Netherlands (R.B.), Department of Radiation Oncology, University Hospital Zurich, University of Zurich, Zurich, Switzerland (M.B., M.G., S.T.L.), Fondazione Policlinico Universitario "A. Gemelli" IRCCS, Rome, Italy (L.B., N.D., R.G., J.L., V.V.), Imagerie Moléculaire In Vivo, CEA, Inserm, Univ Paris Sud, CNRS, Université

Paris Saclay, Orsay, France (I.B., C.N., F.O.), Cancer Imaging Dept, School of Biomedical Engineering and Imaging Sciences, King's College London, London, United Kingdom (G.J.R.C., V.G., M.M.S.), Department of Nuclear Medicine and Molecular Imaging, Lausanne University Hospital, Lausanne, Switzerland (A.D.), Laboratory of Medical Information Processing (LaTIM) - team ACTION (image-guided therapeutic action in oncology), INSERM, UMR 1101, IBSAM, UBO, UBL, Brest, France (M.C.D., M.H., T.U.), Department of Radiation Oncology, the Netherlands Cancer Institute (NKI), Amsterdam, The Netherlands (C.V.D.), Department of Radiology, Stanford University School of Medicine, Stanford (CA), USA (S.E., S.N.), Department of Radiation Oncology, Physics Division, University of Michigan, Ann Arbor (MI), USA (I.E.N., A.U.K.R.), Surgical Planning Laboratory, Brigham and Women's Hospital and Harvard Medical School, Harvard University, Boston (MA), USA (A.Y.F.), Department of Cancer Imaging and Metabolism, Moffitt Cancer Center, Tampa (FL), USA (R.J.G.), Department of Medical Image Computing, German Cancer Research Center (DKFZ), Heidelberg, Germany (M.G., F.I., K.H.M.H., J.S.), The D-Lab, Department of Precision Medicine, GROW-School for Oncology and Developmental Biology, Maastricht University Medical Centre+, Maastricht, The Netherlands (P.L., R.T.H.L.), Section for Biomedical Physics, Department of Radiation Oncology, University of Tübingen, Germany (F.L., J.S.F., D.T.), Department of Clinical Medicine, University of Bergen, Bergen, Norway (A.L.), Department of Radiation Oncology, University of California, San Francisco (CA), USA (O.M.), University of Geneva, Geneva, Switzerland (H.M.), Department of Electrical Engineering, Stanford University, Stanford (CA), USA (S.N.), Department of Medicine (Biomedical Informatics Research), Stanford University School of Medicine, Stanford (CA), USA (S.N.), Departments of Radiology and Physics, University of British Columbia, Vancouver (BC), Canada (A.R.), Department of Computational Medicine and Bioinformatics, University of Michigan, Ann Arbor (MI), USA (A.U.K.R.), Department of Radiation Oncology, University of Groningen, University Medical Center Groningen (UMCG), Groningen, The Netherlands (N.M.S., R.J.H.M.S., L.V.D.), School of Engineering, Cardiff University, Cardiff, United Kingdom (E.S.,

P.W.), Department of Medical Physics, Velindre Cancer Centre, Cardiff, United Kingdom (E.S.), Department of Radiotherapy and Radiation Oncology, Faculty of Medicine and University Hospital Carl Gustav Carus, Technische Universität Dresden, Dresden, Germany (E.G.C.T., C.R., S.Lö), Helmholtz-Zentrum Dresden - Rossendorf, Institute of Radiooncology – OncoRay, Dresden, Germany (E.G.C.T., C.R.), Department of Nuclear Medicine, CHU Milétrie, Poitiers, France (T.U.), Department of Radiology, the Netherlands Cancer Institute (NKI), Amsterdam, The Netherlands (J.G.), GROW-School for Oncology and Developmental Biology, Maastricht University Medical Center, Maastricht, The Netherlands (J.G.), Department of Radiation Oncology, Dana-Farber Cancer Institute, Brigham and Women's Hospital, Harvard Medical School, Boston (MA), USA (J.G.), Department of Radiology, Leiden University Medical Center (LUMC), Leiden, The Netherlands (F.H.P.V.)

Corresponding author

Alex Zwanenburg, mail: alexander.zwanenburg@nct-dresden.de, tel: +493514587442, National Center for Tumor Diseases, partner site Dresden, and OncoRay - National Center for Radiation Research in Oncology, Fetscherstr. 74, PF 41, 01307 Dresden, Germany

Funding information

The authors received funding from the Cancer Research UK and Engineering and Physical Sciences Research Council, with the Medical Research Council and the Department of Health & Social Care (C1519/A16463: M.M.S., G.C., V.G.), Dutch Cancer Society (10034: R.B.), EU 7th framework program (ARTFORCE 257144: R.T.H.L., P.L.; REQUITE 601826: R.T.H.L., P.L.), Engineering and Physical Sciences Research Council (EP/M507842/1: P.W., E.S.; EP/N509449/1: P.W., E.S.), European Research Council (ERC AdG-2015: 694812-Hypoximmuno: R.T.H.L., P.L.; ERC StG-2013: 335367 bio-iRT: D.T.), Eurostars (DART 10116: R.T.H.L., P.L.; DECIDE 11541: R.T.H.L., P.L.), French National Institute of Cancer (C14020NS:

M.C.D., M.H.), French National Research Agency (ANR-10-LABX-07-01: M.C.D., M.H.; ANR-11-IDEX-0003-02: C.N., F.O., I.B.), German Federal Ministry of Education and Research (BMBF-03Z1N52: A.Z., S.Le, E.G.C.T, C.R.), Horizon 2020 Framework Programme (BD2Decide PHC-30-689715: R.T.H.L., P.L.; IMMUNOSABR SC1-PM-733008: R.T.H.L., P.L.), Innovative Medicines Initiative (IMI JU QuIC-ConCePT 115151: R.T.H.L., P.L.), Interreg V-A Euregio Meuse-Rhine (Euradiomics: R.T.H.L., P.L.), National Cancer Institute (P30CA008748: A.A.; U01CA187947: S.E., S.N.; U24CA189523: S.B., S.P., S.M.H., C.D.), National Institute of Neurological Disorders and Stroke (R01NS042645: S.B., S.P., S.M.H., C.D.), National Institutes of Health (R01CA198121: A.A.; U01CA143062: R.J.G.; U01CA190234: J.G., A.Y.F., H.J.W.L.A.; U24CA180918: A.Y.F.; U24CA194354: J.G., A.Y.F., H.J.W.L.A.), SME phase 2 (RAIL 673780: R.T.H.L., P.L.), Swiss National Science Foundation (310030 173303: M.B., S.T.L., M.G.; PZ00P2 154891: A.D.), Technology Foundation STW (10696 DuCAT: R.T.H.L., P.L.; P14-19 Radiomics STRaTegy: R.T.H.L., P.L.), The Netherlands Organisation for Health Research and Development (10-10400-98-14002: R.B.), The Netherlands Organisation for Scientific Research (14929: E.A.G.P., R.B.), University of Zurich Clinical Research Priority Program (Tumor Oxygenation: M.B., S.T.L., M.G.), and the Wellcome Trust (WT203148/Z/16/Z: M.M.S., G.C., V.G.).

Manuscript Type

Original research

Word Count for Text

270 (abstract)

2780 (main text)

Title: The Image Biomarker Standardization Initiative: standardized quantitative radiomics for high-throughput image-based phenotyping

Article Type: Original research

Summary statement:

The Image Biomarker Standardization Initiative validated consensus-based reference values for 169 radiomics features, thus enabling calibration and verification of radiomics software.

Key results:

- 25 research teams found agreement for calculation of 169 radiomics features derived from a digital phantom and a human lung cancer on CT scan.
- Of these 169 candidate radiomics features, good to excellent reproducibility was achieved for 167 radiomics features using MRI, 18F-FDG PET and CT images obtained in 51 patients with soft-tissue sarcoma.

Keywords

Radiomics, standardization, software quality assurance, quantitative image analysis, reporting guidelines

Abbreviations

2D: Two-dimensional

3D: Three-dimensional

GTV: gross tumor volume

IBSI: Image Biomarker Standardization Initiative

ICC: intra-class correlation coefficient

ROI: region of interest

1
2
3
4
5
6
7
8
9
10
11
12
13
14
15
16
17
18
19
20
21
22
23
24
25
26
27
28
29
30
31
32
33
34
35
36
37
38
39
40
41
42
43
44
45
46
47
48
49
50
51
52
53
54
55
56
57
58
59
60

Abstract

Background: Radiomic features may quantify characteristics present in medical imaging. However, the lack of standardized definitions and validated reference values have hampered clinical usage.

Purpose: To standardize a set of 174 radiomic features.

Materials and Methods: Radiomic features were assessed in three phases. In phase I, 487 features were derived from the basic set of 174 features. Twenty-five research teams with unique radiomics software implementations computed feature values directly from a digital phantom, without any additional image processing. In phase II, fifteen teams computed values for 1347 derived features using a CT image of a patient with lung cancer and predefined image processing configurations. In both phases, consensus among the teams on the validity of tentative reference values was measured through the frequency of the modal value: <3 matches: weak; 3-5: moderate; 6-9: strong; ≥10 very strong. In the final phase (III), a public dataset of multi-modality imaging (CT, 18F-FDG-PET and T1-weighted MR) from 51 patients with soft-tissue sarcoma was used to prospectively assess reproducibility of standardized features..

Results: Consensus on reference values was initially weak for 232/302 (76.8%; phase I) and 703/1075 (65.4%; phase II) features. At the final iteration, weak consensus remained for only 2/487 (0.4%; phase I) and 19/1347 (1.4%; phase II) features, and strong or better consensus was achieved for 463/487 (95.1%; phase I) and 1220/1347 (90.6%; phase II). Overall, 169/174 features were standardized in the first two phases. In the final validation phase (III), almost all standardized features could be excellently reproduced: CT:166/169 features; PET:164/169 and MRI: 164/169.

Conclusion: A set of 169 radiomics features was standardized, which enables verification and calibration of different radiomics software.

Introduction

Personalization of medicine is driven by the need to accurately diagnose and define suitable treatments for patients (1). Medical imaging is a potential source of biomarkers, by providing a macroscopic view of tissues of interest (2). Imaging has the advantage of being non-invasive, readily available in clinical care, and repeatable (3,4).

Radiomics extracts features from medical imaging that quantify its phenotypic characteristics in an automated, high-throughput manner (5). Such features may prognosticate, predict treatment outcomes, and assess tissue malignancy in cancer research (6–9). In neuroscience, features may detect Alzheimer's disease (10) and diagnose autism spectrum disorder (11).

Despite the growing clinical interest in radiomics, published studies have been difficult to reproduce and validate (5,9,12–14). Even for the same image, two different software implementations will often produce different feature values. This is because standardized definitions of radiomics features with verifiable reference values are lacking, and the image processing schemes required to compute features are not implemented consistently (15–18). This is exacerbated by reporting that is insufficiently detailed to enable studies and findings to be reproduced (19).

We formed the Image Biomarker Standardization Initiative (IBSI) to address these challenges by fulfilling the following objectives: I) to establish a nomenclature and definitions for commonly used radiomics features; II) to establish a general radiomics image processing scheme for calculation of features from imaging; III) to provide datasets and associated reference values for verification and calibration of software implementations for image

1
2
3
4
5
6
7
8
9
10
11
12
13
14
15
16
17
18
19
20
21
22
23
24
25
26
27
28
29
30
31
32
33
34
35
36
37
38
39
40
41
42
43
44
45
46
47
48
49
50
51
52
53
54
55
56
57
58
59
60

processing and feature computation; and IV) to provide a set of reporting guidelines for studies involving radiomic analyses.

Materials and Methods

Study Design

We divided the current work into three phases (Figure 1). The first two phases focussed on iterative standardization and were followed by a third validation phase. In phase I, the main objective was to standardize radiomics feature definitions and define reference values, in the absence of any additional image processing. In phase II, we defined a general radiomics image processing scheme and obtained reference values for features under different image processing configurations. In phase III, we assessed if the standardization conducted in the previous phases resulted in reproducible feature values for a validation dataset.

Research teams

We invited teams of radiomics researchers to collaborate in the IBSI. Participation was voluntary and open for the duration of the study. Teams were eligible if they:

- developed their own software for image processing and feature computation;
- could participate in any phase of the study.

Radiomics features

We defined set of 174 radiomics features (Table 1). This set consisted of features that are commonly used to quantify the morphology, first-order statistical aspects, and spatial relationships between voxels (texture) in regions of interest in 3D images. Texture features have additional, feature-specific parameters that are required to compute them, which increased the number of computed features beyond 174 (supplementary note A). All feature

1
2
3 definitions are provided in chapter 3 of the IBSI reference manual (online supplemental
4 materials).
5
6
7

8 9 *General radiomics image processing scheme*

10
11 We defined a general radiomics image processing scheme based on descriptions in the
12 literature (3,6,17,20). The scheme contained the main processing steps required for
13 computation of features from a reconstructed image, and is depicted in Figure 2. A full
14 description of these image processing steps may be found in chapter 2 of the IBSI reference
15 manual (online supplemental materials).
16
17
18
19
20
21
22

23 24 *Datasets*

25
26 Each phase used a different dataset. In phase I, we designed a small 80-voxel three-
27 dimensional digital phantom with a 74-voxel region of interest (ROI) mask to facilitate the
28 process of establishing reference values for features, without involving image processing.
29
30
31
32
33

34
35 In phase II we used a publicly available CT image of a lung cancer patient. The
36 accompanying segmentation of the gross tumor volume (GTV) was used as the ROI (21).
37
38
39
40

41 The validation dataset that was used in phase III consisted of a cohort of 51 patients with
42 soft-tissue sarcoma and multi-modality imaging (co-registered CT, 18F-FDG PET and T1-
43 weighted MRI) from the Cancer Imaging Archive (20,22,23). Each image was accompanied
44 by a GTV segmentation, which was used as the ROI. PET and MRI were centrally pre-
45 processed (supplementary note B) to ensure that SUV-conversion and bias-field correction
46 steps did not affect validation.
47
48
49
50
51
52
53
54
55
56
57
58
59
60

Defining consensus on the validity of feature reference values

In the first two phases, research teams computed feature values from the ROI in the associated image dataset directly (phase I) and according to predefined image processing parameters (phase II; supplementary note B). All of the most recent values submitted by each team were collected and limited to three significant digits. Then, we used the mode of the submitted values for each feature as a tentative reference value.

We quantified the level of consensus on the validity of a tentative reference value for each feature using two measures:

1. The number of research teams that submitted a value that matched the tentative reference value within a tolerance margin (supplementary note C).
2. The above number divided by the total number of research teams that submitted a value.

Four consensus levels were assigned based on the first consensus measure: <3: weak; 3-5: moderate; 6-9: strong; ≥ 10 : very strong. The second measure assessed the stability of the consensus. We considered a tentative reference value for a feature to be valid only if it had at least moderate consensus and it was reproduced by an absolute majority (exceeding 50%) of the contributing research teams.

Iterative standardization process

In the first two phases, we iteratively refined consensus on the validity of feature reference values. This iterative process simultaneously served to standardize feature definitions and the general radiomics image processing scheme (24). At the start of the iterative process we provided initial definitions for features (phase I) and the general radiomics image processing scheme (phase II) in a working document. For phase I, we moreover manually calculated mathematically exact reference values for all but morphological features to verify values

1
2
3 produced by the research teams. For phase II, we defined five different image processing
4 configurations (A-E) that covered a range of image processing parameters and methods that
5 are commonly used in radiomics studies (supplementary note B).
6
7
8
9

10
11 After producing the initial working document, we asked the research teams to compute
12 feature values from the ROI in the digital phantom (phase I) and from the ROI in the lung
13 cancer CT image after image processing according to the different predefined image
14 processing configurations (phase II). Feature values were collected and processed to
15 analyze the consensus on the validity of tentative reference values. The results were then
16 made available to all teams at an average interval of 4 weeks. The study leader would also
17 contact the teams with feedback after comparing their submitted feature values with the
18 mathematically exact values (phase I only) and with feature values obtained by other teams
19 (phases I and II). The research teams provided feedback in the form of questions and
20 suggestions concerning the standardization of radiomics software and regarding descriptions
21 in the working document. The working document was regularly updated as a result. Teams
22 would then make changes to their software based on the results of the analysis and
23 feedback from the study leader.
24
25
26
27
28
29
30
31
32
33
34
35
36
37
38
39
40

41 The two iterative phases were staggered to make it easier to separate differences and errors
42 related to feature computation from those related to image processing. The initial
43 contributions from phase I were analyzed in September 2016. We initiated phase II after
44 moderate or better consensus on the validity of reference values was achieved for at least
45 70% of the features, i.e. time point 6 (January 2017). Initial contributions for phase II were
46 analyzed at time point 10 (April 2017). Afterwards, phases I and II were concurrent. We
47 halted the iterative standardization process at time point 25 (March 2019) after we attained
48 strong or better consensus on validity of reference values for over 90% of the features in
49 both phases I and II. The overall timeline of the study is summarized in supplementary note
50 D.
51
52
53
54
55
56
57
58
59
60

Validation

After the standardization process finished, we asked the research teams to compute 174 features from the GTV in each of the images in the soft-tissue sarcoma validation cohort using a realistic, pre-defined image processing configuration (supplementary note B). The computed feature values were collected and processed centrally, as follows. First, for each team we removed any feature that was not standardized by their software. To do so, we compared the reference values of the respective feature with the values that the team obtained from the CT image of the lung cancer patient under image processing configurations C, D and E (as in phase II). If a value did not match its reference value, the feature was not used. The reproducibility of remaining, standardized features was subsequently assessed using a two-way random effects, single rater, absolute agreement intraclass correlation coefficient (ICC) (25). Using the lower boundary of the 95% confidence interval of the ICC value (ICC-CI-low) (26), reproducibility of each feature was assigned to one of the following categories, after Koo and Li (27): poor: $ICC-CI-low < 0.50$; moderate: $0.50 \leq ICC-CI-low < 0.75$; good: $0.75 \leq ICC-CI-low < 0.90$; excellent: $0.90 \leq ICC-CI-low$.

Results

Characteristics of the participating research teams

Twenty-five teams contributed to the IBSI (Figure 3; supplementary note E). Fifteen teams contributed to both standardization phases, and nine teams contributed to the validation phase. One team retired because they switched to software developed by another team. Five teams implemented 95% or more of the defined features. Nine teams were able to compute features for all image processing configurations in phase II (supplementary note F).

Two top-level institutions (e.g. university) provided more than one participating team of researchers, i.e. the University Medical Center Groningen and INSERM Brest with three and

two teams respectively. This did not compromise consensus on the validity of feature reference values. Moderate, strong or very strong consensus on the validity of the reference values was based on teams from at least three, five and eight different top-level institutions, respectively (see supplementary note G).

MATLAB ($n=10$), C++ ($n=7$) and Python ($n=5$) were the most popular programming languages. No language dependency was found: consensus of all features with a moderate or better consensus on the validity of their reference values were based on multiple programming languages (see supplementary note H).

Consensus on validity of feature reference values

Consensus on the validity of feature reference values improved over the course of the study, as shown in Figure 4 and Table 2. Initially, only weak consensus existed for the majority of features: 232/302 (76.8%) and 703/1075 (65.4%) for phase I and II, respectively.

At the final analysis time point, the number of features with a weak consensus had decreased to 2/487 (0.4%) for phase I and 19/1347 (1.4%) for phase II. The remaining features with weak consensus on the validity of their (tentative) reference values were the area and volume densities of the oriented minimum bounding box and the minimum volume enclosing ellipsoid (see supplementary note I). We were unable to standardize the complex algorithms that are required to compute the oriented minimum bounding box and minimum volume enclosing ellipsoid. Therefore, the above features should not be regarded as standardized.

As shown in Table 2, strong or better consensus could be established for 463/487 (95.1%) and 1220/1347 (90.6%) features in phases I and II respectively. None of these features were found to be unstable. In phase II, 2/108 (1.9%) features with moderate consensus were

1
2
3
4
5
6
7
8
9
10
11
12
13
14
15
16
17
18
19
20
21
22
23
24
25
26
27
28
29
30
31
32
33
34
35
36
37
38
39
40
41
42
43
44
45
46
47
48
49
50
51
52
53
54
55
56
57
58
59
60

unstable. Both were derived from the same feature: the area under the curve of the intensity-volume histogram. Hence, we do not consider this feature to be standardized.

The most commonly implemented features were mean, skewness, excess kurtosis and minimum of the intensity-based statistics family. These were implemented by 23/24 research teams. No feature was implemented by all teams (see supplementary note J).

Reproducibility of standardized features

We were able to find stable reference values with moderate or better consensus for 169/174 features. In the validation phase, most of these features could be reproduced well (Figure 5, supplementary note K). Excellent reproducibility was found for 166/174, 164/174 and 164/174 features for CT, PET and MRI, respectively, and good reproducibility was found for 1/174, 3/174 and 3/174 features. For each modality, 2/174 features had unknown reproducibility, indicating that they were computed by less than two teams during validation. These features were Moran’s I index and Geary’s C measure, which although they were standardized, are expensive to compute. The remaining 5/174 features could not be standardized during the first two phases and were not assessed during validation.

Discussion

In this study, the Image Biomarker Standardization Initiative produced and validated a set of consensus-based reference values for radiomics features. Twenty-five research teams were able to standardize 169/174 features, which were subsequently shown to have good to excellent reproducibility in a validation data set.

With the completion of the current work, compliance with the IBSI standard can be checked for any radiomics software, as follows:

- Use the software to compute features using the digital phantom. Compare the resulting values against the reference values that are found in the IBSI reference manual and the compliance check spreadsheet created for this purpose (online supplemental materials). Investigate any difference. Subsequently, resolve the differences or explain them, e.g. the use of kurtosis instead of excess kurtosis.
- Afterwards, repeat the above with the CT dataset used in this study and one or more of the image processing configurations that were used in phase II.

Initial consensus on the validity of reference values for many features was weak, which means that teams obtained different values for the same feature. This mirrors findings reported elsewhere (15–18). Several notable causes of deviations were identified – for example, differences in interpolation, morphological representation of the ROI and nomenclature differences – and subsequently resolved (supplementary note L). In effect, we cross-calibrated radiomics software implementations.

The demonstrated lack of initial correspondence between teams carries a clinical implication. Software implementations of seemingly well-defined mathematical formulas can vary greatly in the numeric results they produce. Clinical radiologists that are using advanced image analysis workstations should be aware of this, think critically about comparing results produced by different workstations and demand more details and validation studies from the vendors of those workstations.

Findings from most radiomics studies have not been translated into clinical practice, and require external retrospective and prospective validation in clinical trials (2,28). The IBSI, in addition to the presented work, has defined reporting guidelines (see supplemental materials) that indicate the elements that should be reported to facilitate this process. However, we refrained from creating a comprehensive recommendation on how to perform a good radiomics analysis, for several reasons. First, such recommendations will necessarily

1
2
3
4
5
6
7
8
9
10
11
12
13
14
15
16
17
18
19
20
21
22
23
24
25
26
27
28
29
30
31
32
33
34
35
36
37
38
39
40
41
42
43
44
45
46
47
48
49
50
51
52
53
54
55
56
57
58
59
60

have to be modality-specific and possibly entity-specific (29,30). The related specific evidence for the effect of particular parameters, e.g. the choice of interpolation algorithm, is far from complete. Secondly, recommendations or guidelines regarding parts of the radiomics analysis are already covered comprehensively elsewhere, e.g. by the TRIPOD statement on diagnostic and prognostic modelling (31). Certainly, the image processing configurations used in phase II are not intended for general use, as their primary aim was to cover a range of different methods. Only the configurations defined for the validation dataset resemble a realistic set of parameters given the entity and the imaging modalities.

The current work has several limitations. First, our aim was to lay a foundation for standardized computation of radiomics features. To this end, we sought to standardize 174 commonly used features, and obtain reference values using image processing methods that radiomics researchers most commonly employ. To keep the scope manageable, many other features such as fractals and image filters were not assessed (32), important modality-specific image processing steps were not benchmarked, and uncommon image processing methods were not investigated either. This is a serious limitation, and one that the IBSI is currently addressing.

Despite the fact that standardized feature computation is an important step towards reproducible radiomics, the need for standardization and harmonization related to image acquisition, reconstruction and segmentation remains, as these constitute additional sources of variability in radiomics studies. Because of this variability, features that can be reproduced from the same image using standardized radiomics software, may nevertheless lack reproducibility in multi-centric or multi-scanner settings (14,19,33). We did not address these issues here as their comprehensive harmonization is the ongoing focus of other consortia and professional societies (2). Other approaches have also been proposed to deal with these issues, such as the reduction of cohort effects on radiomics features using statistical

methods (34) and application of artificial intelligence to convert between reconstruction kernels in CT imaging (35).

In conclusion, the Image Biomarker Standardization Initiative was able to produce and validate reference values for radiomics features. These reference values enable verification of radiomics software, which will increase reproducibility of radiomics studies and facilitate clinical translation of radiomics.

References

1. La Thangue NB, Kerr DJ. Predictive biomarkers: a paradigm shift towards personalized cancer medicine. *Nat Rev Clin Oncol*. 2011;8(10):587–596.
2. O'Connor JPB, Aboagye EO, Adams JE, et al. Imaging biomarker roadmap for cancer studies. *Nat Rev Clin Oncol*. 2017;14(3):169–186.
3. Lambin P, Leijenaar RTH, Deist TM, et al. Radiomics: the bridge between medical imaging and personalized medicine. *Nat Rev Clin Oncol*. 2017;14(12):749–762.
4. Morin O, Vallières M, Jochems A, et al. A Deep Look Into the Future of Quantitative Imaging in Oncology: A Statement of Working Principles and Proposal for Change. *Int J Radiat Oncol Biol Phys*. 2018;102(4):1074–1082.
5. Gillies RJ, Kinahan PE, Hricak H. Radiomics: Images Are More than Pictures, They Are Data. *Radiology*. 2016;278(2):563–577.
6. Aerts HJWL, Velazquez ER, Leijenaar RTH, et al. Decoding tumour phenotype by noninvasive imaging using a quantitative radiomics approach. *Nat Commun*. 2014;5:4006.
7. Sun R, Limkin EJ, Vakalopoulou M, et al. A radiomics approach to assess tumour-infiltrating CD8 cells and response to anti-PD-1 or anti-PD-L1 immunotherapy: an imaging biomarker, retrospective multicohort study. *Lancet Oncol*. 2018;19(9):1180–1191.
8. Lu H, Arshad M, Thornton A, et al. A mathematical-descriptor of tumor-mesoscopic-structure from computed-tomography images annotates prognostic- and molecular-phenotypes of epithelial ovarian cancer. *Nat Commun*. 2019;10(1):764.
9. Bodalal Z, Trebeschi S, Nguyen-Kim TDL, Schats W, Beets-Tan R. Radiogenomics: bridging imaging and genomics. *Abdom Radiol*. 2019;44(6):1960–1984.
10. Leandrou S, Petroudi S, Kyriacou PA, Reyes-Aldasoro CC, Pattichis CS. Quantitative MRI Brain Studies in Mild Cognitive Impairment and Alzheimer's Disease: A Methodological Review. *IEEE Rev Biomed Eng*. 2018;11:97–111.
11. Chaddad A, Desrosiers C, Toews M. Multi-scale radiomic analysis of sub-cortical regions in MRI related to autism, gender and age. *Sci Rep*. 2017;7:45639.
12. Berenguer R, Pastor-Juan MDR, Canales-Vázquez J, et al. Radiomics of CT Features May Be Nonreproducible and Redundant: Influence of CT Acquisition Parameters. *Radiology*. 2018;288(2):407–415.

13. Welch ML, McIntosh C, Haibe-Kains B, et al. Vulnerabilities of radiomic signature development: The need for safeguards. *Radiother Oncol*. 2019;130:2–9.
14. Meyer M, Ronald J, Vernuccio F, et al. Reproducibility of CT Radiomic Features within the Same Patient: Influence of Radiation Dose and CT Reconstruction Settings. *Radiology*. 2019;190928.
15. Kalpathy-Cramer J, Mamomov A, Zhao B, et al. Radiomics of Lung Nodules: A Multi-Institutional Study of Robustness and Agreement of Quantitative Imaging Features. *Tomography*. 2016;2(4):430–437.
16. Bogowicz M, Leijenaar RTH, Tanadini-Lang S, et al. Post-radiochemotherapy PET radiomics in head and neck cancer - The influence of radiomics implementation on the reproducibility of local control tumor models. *Radiother Oncol*. 2017;125(3):385–391.
17. Hatt M, Tixier F, Pierce L, Kinahan PE, Le Rest CC, Visvikis D. Characterization of PET/CT images using texture analysis: the past, the present... any future? *Eur J Nucl Med Mol Imaging*. 2017;44(1):151–165.
18. Foy JJ, Robinson KR, Li H, Giger ML, Al-Hallaq H, Armato SG. Variation in algorithm implementation across radiomics software. *J Med Imaging*. 2018;5(4):044505.
19. Traverso A, Wee L, Dekker A, Gillies R. Repeatability and Reproducibility of Radiomic Features: A Systematic Review. *Int J Radiat Oncol Biol Phys*. 2018;102(4):1143–1158.
20. Vallières M, Freeman CR, Skamene SR, El Naqa I. A radiomics model from joint FDG-PET and MRI texture features for the prediction of lung metastases in soft-tissue sarcomas of the extremities. *Phys Med Biol*. 2015;60(14):5471–5496.
21. Lambin P. Radiomics Digital Phantom. 2016.<http://dx.doi.org/10.17195/candat.2016.08.1>.
22. Clark K, Vendt B, Smith K, et al. The Cancer Imaging Archive (TCIA): maintaining and operating a public information repository. *J Digit Imaging*. 2013;26(6):1045–1057.
23. Vallières M, Freeman CR, Skamene SR, El Naqa I. Data from: A radiomics model from joint FDG-PET and MRI texture features for the prediction of lung metastases in soft-tissue sarcomas of the extremities. The Cancer Imaging Archive; 2015.<http://dx.doi.org/10.7937/K9/TCIA.2015.7GO2GSKS>.
24. Diamond IR, Grant RC, Feldman BM, et al. Defining consensus: a systematic review recommends methodologic criteria for reporting of Delphi studies. *J Clin Epidemiol*. 2014;67(4):401–409.
25. Shrout PE, Fleiss JL. Intraclass correlations: uses in assessing rater reliability. *Psychol Bull*. psycnet.apa.org; 1979;86(2):420–428.
26. McGraw KO, Wong SP. Forming inferences about some intraclass correlation coefficients. *Psychol Methods*. doi.apa.org; 1996;1(1):30–46.
27. Koo TK, Li MY. A guideline of selecting and reporting intraclass correlation coefficients for reliability research. *J Chiropr Med*. 2016;15(2):155–163.
28. Sollini M, Antunovic L, Chiti A, Kirienko M. Towards clinical application of image mining: a systematic review on artificial intelligence and radiomics. *Eur J Nucl Med Mol Imaging*. 2019;<https://doi.org/10.1007/s00259-019-04372-x>.
29. Orlhac F, Soussan M, Maisonobe J-A, Garcia CA, Vanderlinden B, Buvat I. Tumor texture analysis in 18F-FDG PET: relationships between texture parameters, histogram indices, standardized uptake values, metabolic volumes, and total lesion glycolysis. *J Nucl Med*. 2014;55(3):414–422.
30. van Timmeren JE, Leijenaar RTH, van Elmpt W, et al. Test-Retest Data for Radiomics Feature Stability Analysis: Generalizable or Study-Specific? *Tomography*. 2016;2(4):361–365.

31. Collins GS, Reitsma JB, Altman DG, Moons KGM. Transparent Reporting of a multivariable prediction model for Individual Prognosis Or Diagnosis (TRIPOD): the TRIPOD Statement. *Br J Surg*. 2015;102(3):148–158.
32. Depeursinge A, Foncubierta-Rodriguez A, Van De Ville D, Müller H. Three-dimensional solid texture analysis in biomedical imaging: review and opportunities. *Med Image Anal*. 2014;18(1):176–196.
33. Zwanenburg A. Radiomics in nuclear medicine: robustness, reproducibility, standardization, and how to avoid data analysis traps and replication crisis. *Eur J Nucl Med Mol Imaging*. 2019;<http://dx.doi.org/10.1007/s00259-019-04391-8>.
34. Orlhac F, Frouin F, Nioche C, Ayache N, Buvat I. Validation of A Method to Compensate Multicenter Effects Affecting CT Radiomics. *Radiology*. 2019;182023.
35. Choe J, Lee SM, Do K-H, et al. Deep Learning-based Image Conversion of CT Reconstruction Kernels Improves Radiomics Reproducibility for Pulmonary Nodules or Masses. *Radiology*. 2019;292(2):365–373.

1
2
3
4
5
6
7
8
9
10
11
12
13
14
15
16
17
18
19
20
21
22
23
24
25
26
27
28
29
30
31
32
33
34
35
36
37
38
39
40
41
42
43
44
45
46
47
48
49
50
51
52
53
54
55
56
57
58
59
60

Figure Legends

Figure 1. Study overview.

The workflow in a typical radiomics analysis starts with acquisition and reconstruction of a medical image. Subsequently, the image is segmented to define regions of interest. Afterwards, radiomics software is used to process the image, and compute features that characterize a region of interest. We focused on standardizing the image processing and feature computation steps. Standardization was performed within two iterative phases. In phase I, we used a specially designed digital phantom to obtain reference values for radiomics features directly. Subsequently, in phase II, a publicly available CT image of a lung cancer patient was used to obtain reference values for features under predefined configurations of a standardized general radiomics image processing scheme. Standardization of image processing and feature computation steps in radiomics software was prospectively validated during phase III by assessing reproducibility of standardized features in a publicly available multi-modality patient cohort of 51 patients with soft-tissue sarcoma.

Figure 2. The general radiomics image processing scheme for computing radiomics features.

Image processing starts with reconstructed images. These images are processed through several optional steps: data conversion (e.g. conversion to Standardized Uptake Values), image post-acquisition processing (e.g. image denoising) and image interpolation. The region of interest (ROI) is either created automatically during the segmentation step or an existing ROI is retrieved. The ROI is then interpolated as well, and intensity and morphological masks are created as copies. The intensity mask may optionally be re-segmented based on intensity values to improve comparability of intensity ranges across a cohort. Radiomics features are then computed from the image masked by the ROI and its immediate neighborhood (local intensity features) or the ROI itself (all others). Image

intensities are moreover discretized prior to computation of features from the intensity histogram (IH), intensity-volume histogram (IVH), grey level co-occurrence matrix (GLCM), grey level run length matrix (GLRLM), grey level size zone matrix (GLSZM), grey level distance zone matrix (GLDZM), neighborhood grey tone difference matrix (NGTDM) and neighboring grey level dependence matrix (NGLDM) families. All processing steps from image interpolation to the computation of radiomics features were evaluated in this study.

Figure 3. Participation and radiomics feature coverage by research teams.

(A) Graph showing the number of research teams at each analysis time point during the two phases of the iterative standardization process. Teams computed features without prior image processing (phase I), and after image processing (phase II), with the aim of finding reference values for a feature. Consensus on the validity of reference values was assessed at each of the analysis time points, the time between which was variable (arbitrary unit; arb. unit). (B) Graph showing the final coverage of radiomics features implemented by each team in phase I, as well as the team's ability to reproduce the reference value of a feature. We were unable to obtain reliable reference values for five features (no ref. value). The teams are listed in supplementary note E.

Figure 4. Iterative development of consensus on the validity of reference values for radiomics features.

We tried to find reliable reference values for radiomics features in an iterative standardization process. In phase I features were computed without prior image processing, whereas in phase II features were assessed after image processing with five predefined configurations (conf. A-E; supplementary note B). The panels show the overall development of consensus on the validity of (tentative) reference values in phases I and II (A) and the development of consensus in phase II, split by image processing configuration (B). Consensus on the validity of a reference value is based on the number of research teams that produce the same value for a feature: weak < 3; moderate: 3-5; strong: 6-9; very strong:

1
2
3
4
5
6
7
8
9
10
11
12
13
14
15
16
17
18
19
20
21
22
23
24
25
26
27
28
29
30
31
32
33
34
35
36
37
38
39
40
41
42
43
44
45
46
47
48
49
50
51
52
53
54
55
56
57
58
59
60

≥ 10. We analyzed consensus at each of the analysis time points, the time between which was variable (arbitrary unit; arb. unit). New features were included at time points 5 and 22, causing an apparent decrease in consensus. For phase II, we first analyzed consensus at time point 10. Image processing configurations C and D were altered after time point 16. Configuration E was altered after revising the re-segmentation processing step at time point 22. See supplementary note D for more information regarding the timeline.

Figure 5. Reproducibility of standardized radiomics features.

We assessed reproducibility of 169 standardized features on a validation cohort of 51 patients with soft-tissue sarcoma and multi-modality imaging (CT, 18F-FDG-PET, T1-weighted MR; shown as CT, PET and MRI), based on the feature values computed by research teams. We assigned each feature to a reproducibility category based on the lower boundary of the 95% confidence interval of the two-way random effects, single rater, absolute agreement intraclass correlation coefficient of the feature: poor: < 0.50; moderate: 0.50-0.75; good: 0.75-0.90; excellent: ≥ 0.90. Five features could not be standardized in this study. Two features with unknown reproducibility were computed by fewer than two teams during validation.

Tables

Table 1. Overview of included radiomics features.

Feature family	Base definition	Number of features			
		Phase I	Phase II conf. A-B (2D)	Phase II conf. C-E (3D)	Phase III
Morphology	29	29	29	29	29
Local intensity	2	2	2	2	2
Intensity-based statistics	18	18	18	18	18
Intensity histogram (IH)	23	23	23	23	23
Intensity-volume histogram (IVH)	7	7	7	7	7
Grey level co-occurrence matrix (GLCM) ^a	25	150	100	50	25
Grey level run-length matrix (GLRLM) ^a	16	96	64	32	16
Grey level size zone matrix (GLSZM) ^a	16	48	32	16	16
Grey level distance zone matrix (GLDZM) ^a	16	48	32	16	16
Neighborhood grey tone difference matrix (NGTDM) ^a	5	15	10	5	5
Neighboring grey level dependence matrix (NGLDM) ^a	17	51	34	17	17
Total	174	487	351	215	174

Note: A set of 174 radiomics features was standardized and validated in three phases. In phase I features were computed without any prior image processing. In phase II features were computed after image processing with five predefined configurations (conf. A-E; supplementary note B). In the final phase III we assessed the reproducibility of features standardized in phases I and II.

^a Texture features have additional parameters that are required for their calculation, which increased the number of computed features (supplementary note A).

Table 2. Consensus on the validity of reference values of radiomics features at initial and final analysis time points for phases I and II.

	total		weak		moderate		Consensus level strong		very strong	≥ mod.	≥ strong
	<i>n</i>	<i>unstable</i>	<i>n</i>	<i>unstable</i>	<i>n</i>	<i>unstable</i>	<i>n</i>	<i>unstable</i>	<i>n</i>	<i>n</i>	<i>n</i>
Initial analysis time point phase I											
phase I	302	147 (48.7)	232 (76.8)	133 (57.3)	48 (15.9)	12 (25.0)	16 (5.3)	2 (12.5)	6 (2.0)	70 (23.2)	22 (7.3)
Initial analysis time point phase II											
phase II	1075	610 (56.7)	703 (65.4)	537 (76.4)	342 (31.8)	73 (21.3)	30 (2.8)	0 (—)	0 (—)	372 (34.6)	30 (2.8)
configuration A	215	28 (13.0)	114 (53.0)	26 (22.8)	98 (45.6)	2 (2.0)	3 (1.4)	0 (—)	0 (—)	101 (47.0)	3 (1.4)
configuration B	215	149 (69.3)	188 (87.4)	149 (79.3)	27 (12.6)	0 (—)	0 (—)	0 (—)	0 (—)	27 (12.6)	0 (—)
configuration C	215	97 (45.1)	87 (40.5)	72 (82.8)	112 (52.1)	25 (22.3)	16 (7.4)	0 (—)	0 (—)	128 (59.5)	16 (7.4)
configuration D	215	162 (75.3)	141 (65.6)	129 (91.5)	63 (29.3)	33 (52.4)	11 (5.1)	0 (—)	0 (—)	74 (34.4)	11 (5.1)
configuration E	215	174 (80.9)	173 (80.5)	161 (93.1)	42 (19.5)	13 (31.0)	0 (—)	0 (—)	0 (—)	42 (19.5)	0 (—)
Final analysis time point phase I & II											
phase I	487	2 (0.4)	2 (0.4)	2 (100.0)	22 (4.5)	0 (—)	234 (48.0)	0 (—)	229 (47.0)	485 (99.6)	463 (95.1)
phase II	1347	20 (1.5)	19 (1.4)	18 (94.7)	108 (8.0)	2 (1.9)	1152 (85.5)	0 (—)	68 (5.0)	1328 (98.6)	1220 (90.6)
configuration A	351	4 (1.1)	4 (1.1)	3 (75.0)	22 (6.3)	1 (4.5)	307 (87.5)	0 (—)	18 (5.1)	347 (98.9)	325 (92.6)
configuration B	351	5 (1.4)	4 (1.1)	4 (100.0)	24 (6.8)	1 (4.2)	317 (90.3)	0 (—)	6 (1.7)	347 (98.9)	323 (92.0)
configuration C	215	4 (1.9)	4 (1.9)	4 (100.0)	9 (4.2)	0 (—)	171 (79.5)	0 (—)	31 (14.4)	211 (98.1)	202 (94.0)
configuration D	215	4 (1.9)	4 (1.9)	4 (100.0)	6 (2.8)	0 (—)	192 (89.3)	0 (—)	13 (6.0)	211 (98.1)	205 (95.3)
configuration E	215	3 (1.4)	3 (1.4)	3 (100.0)	47 (21.9)	0 (—)	165 (76.7)	0 (—)	0 (—)	212 (98.6)	165 (76.7)

Note: Reference values of radiomics features were iteratively obtained in two phases. In phase I features were computed without prior image processing, whereas in phase II features were computed after image processing with five predefined configurations (conf. A-E; supplementary note B). Consensus on the validity of a reference value was based on the number of research teams that produced the same value: weak < 3; moderate (mod.): 3-5; strong: 6-9; very strong: ≥ 10. For each consensus level, the number and percentage of features is shown (“*n*”) together with the number and percentage of these features for which the consensus was only carried by a minority of teams (≤ 50%; “*unstable*”). Features with very strong consensus were never unstable, and the respective column was omitted. The number of features increased between the initial and final time points due to adding new features and computing features with additional feature-specific parameters (supplementary notes A, D).

Supplemental Materials

Supplementary notes

Contains additional information concerning the methodology and results of the current work.

IBSI reference manual

Contains extensive descriptions of the image processing scheme (chapter 2), the feature definitions (chapter 3), reporting guidelines and feature nomenclature (chapter 4), and a description of the datasets with instructions on how to use them (chapter 5).

Compliance check spreadsheet

The compliance check spreadsheet provides the reference values in an accessible manner and enables calibration of software for computing radiomics features. Feature values can be inserted and will automatically be checked against the reference values obtained in this study.

IBSI guidelines for reporting on radiomics studies

A stand-alone copy of the checklist for reporting on radiomics studies.

Datasets

The datasets and corresponding segmentation masks are available in DICOM and NIFTI formats and may be found on the IBSI website: <https://theibsi.github.io>.

Analysis scripts

Analysis scripts (in R) are available on GitHub:

https://github.com/theibsi/ibsi_1_data_analysis

Acknowledgments

The authors wish to thank Baptiste Laurent, Sarah Mattonen, Dr. Hesham Elhalawani, Dr. Jayashree Kalpathy-Cramer, Dr. Dennis Mackin, Ida A. Nissen, Prof. Dr. Dimitris Visvikis and Dr. Maqsood Yaqub for their valuable ideas and support. In addition, we would like to thank Rutu Pandya and Roger Schaer for technical support in setting up and administrating the IBSI website (<https://theibsi.github.io/>). We also would like to thank David Clunie for his input on creating permanent IBSI identifiers and providing a DICOM version of the digital phantom, and Alberto Traverso for integrating the work of the IBSI in the Radiomics Ontology (<https://bioportal.bioontology.org/ontologies/RO/>). We would also wish to extend a special thanks to the European Society for Radiotherapy & Oncology and Prof. Dr. Uulke van der Heide for organizing a Radiomics Mini Workshop where the idea for a standardization initiative was first discussed.

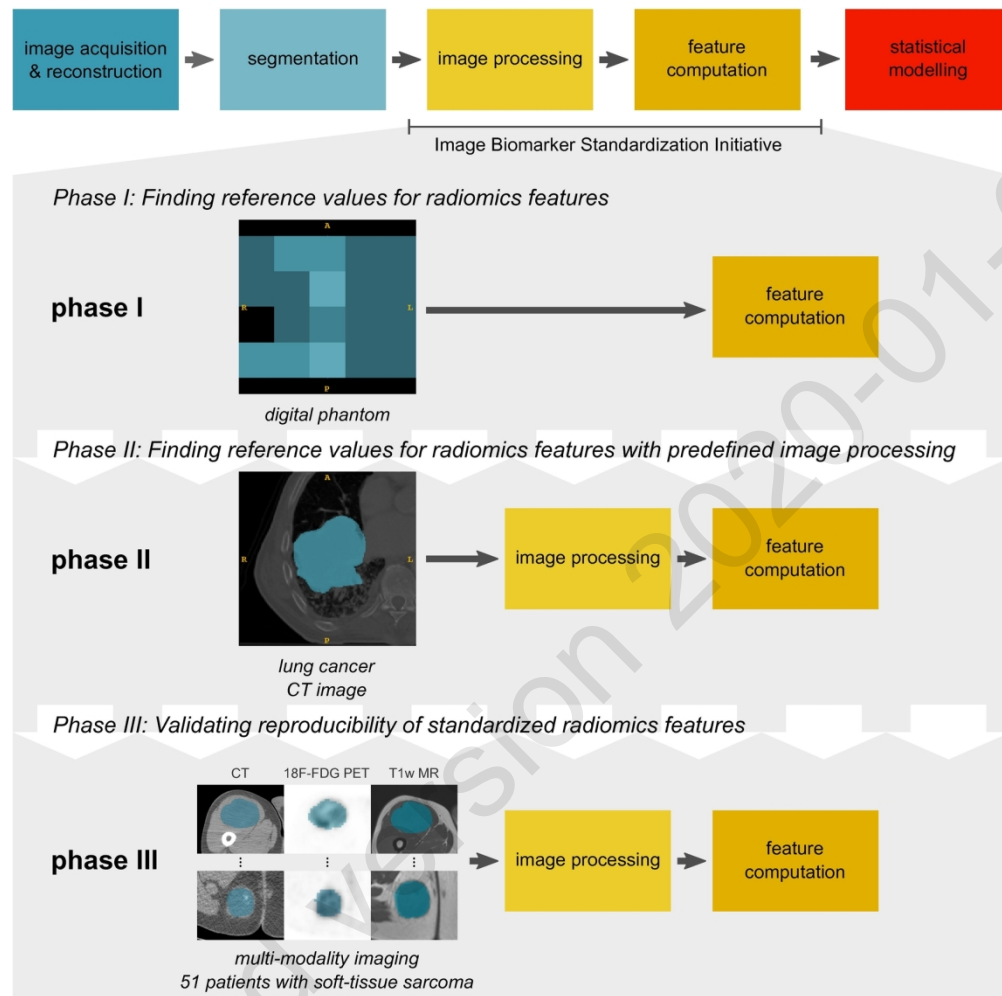
Imaging and radiomics workflow

fig 1 Study overview. The workflow in a typical radiomics analysis starts with acquisition and reconstruction of a medical image. Subsequently, the image is segmented to define regions of interest. Afterwards, radiomics software is used to process the image, and compute features that characterize a region of interest. We focused on standardizing the image processing and feature computation steps. Standardization was performed within two iterative phases. In phase I, we used a specially designed digital phantom to obtain reference values for radiomics features directly. Subsequently, in phase II, a publicly available CT image of a lung cancer patient was used to obtain reference values for features under predefined configurations of a standardized general radiomics image processing scheme. Standardization of image processing and feature computation steps in radiomics software was prospectively validated during phase III by assessing reproducibility of standardized features in a publicly available multi-modality patient cohort of 51 patients with soft-tissue sarcoma.

157x161mm (300 x 300 DPI)

1
2
3
4
5
6
7
8
9
10
11
12
13
14
15
16
17
18
19
20
21
22
23
24
25
26
27
28
29
30
31
32
33
34
35
36
37
38
39
40
41
42
43
44
45
46
47
48
49
50
51
52
53
54
55
56
57
58
59
60

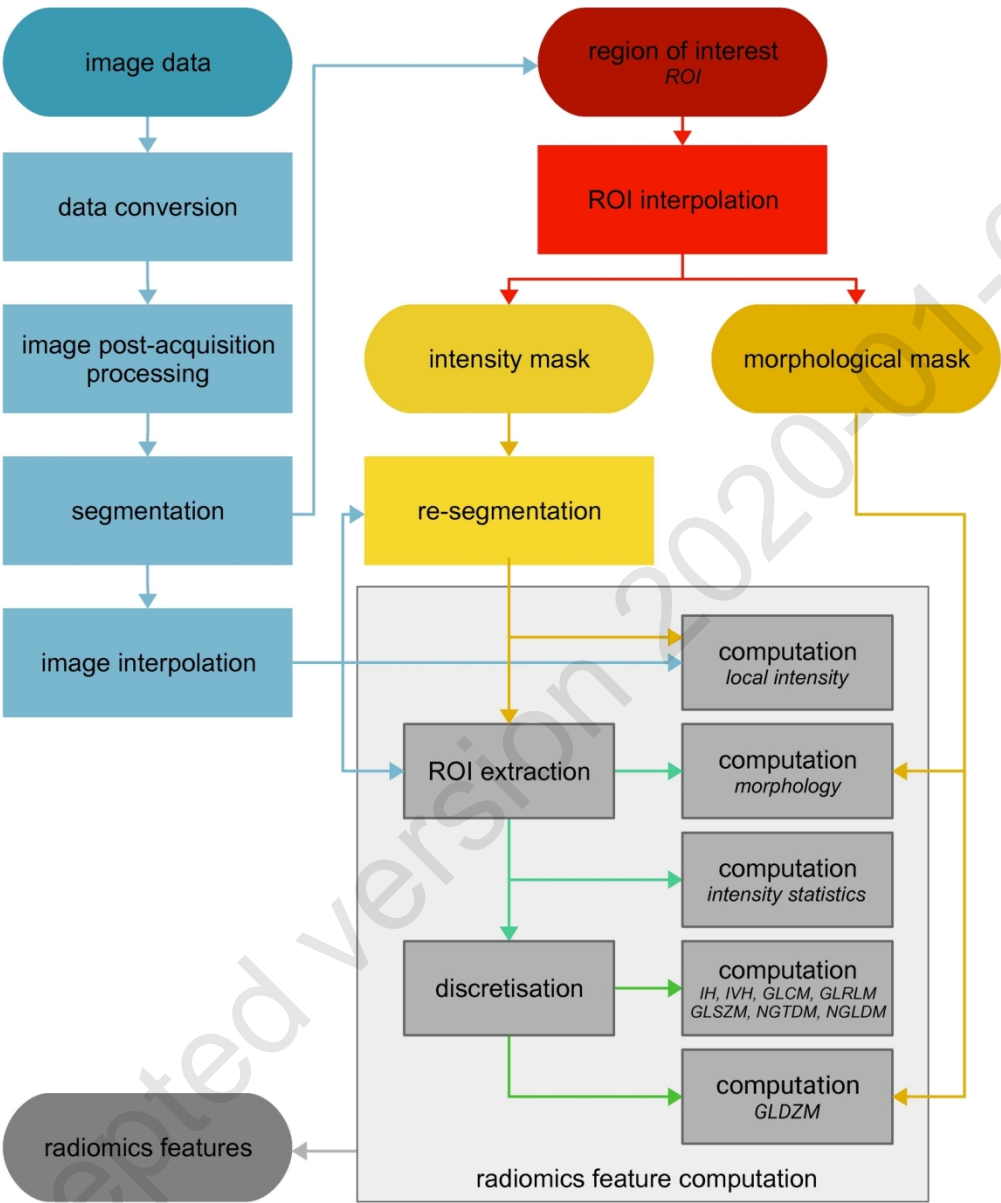


fig 2 The general radiomics image processing scheme for computing radiomics features. Image processing starts with reconstructed images. These images are processed through several optional steps: data conversion (e.g. conversion to Standardized Uptake Values), image post-acquisition processing (e.g. image denoising) and image interpolation. The region of interest (ROI) is either created automatically during the segmentation step or an existing ROI is retrieved. The ROI is then interpolated as well, and intensity and morphological masks are created as copies. The intensity mask may optionally be re-segmented based on intensity values to improve comparability of intensity ranges across a cohort. Radiomics features are then computed from the image masked by the ROI and its immediate neighborhood (local intensity features) or the ROI itself (all others).

138x165mm (300 x 300 DPI)

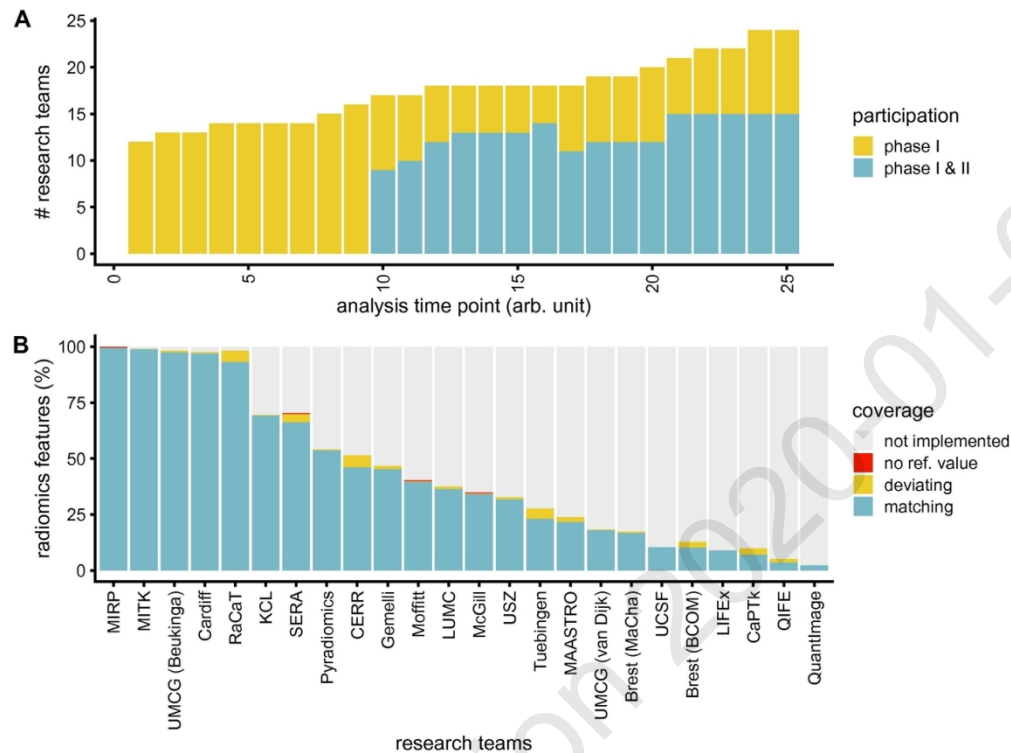


fig 3 Participation and radiomics feature coverage by research teams. (A) Graph showing the number of research teams at each analysis time point during the two phases of the iterative standardization process. Teams computed features without prior image processing (phase I), and after image processing (phase II), with the aim of finding reference values for a feature. Consensus on the validity of reference values was assessed at each of the analysis time points, the time between which was variable (arbitrary unit; arb. unit). (B) Graph showing the final coverage of radiomics features implemented by each team in phase I, as well as the team's ability to reproduce the reference value of a feature. We were unable to obtain reliable reference values for five features (no ref. value). The teams are listed in supplementary note E.

119x88mm (300 x 300 DPI)

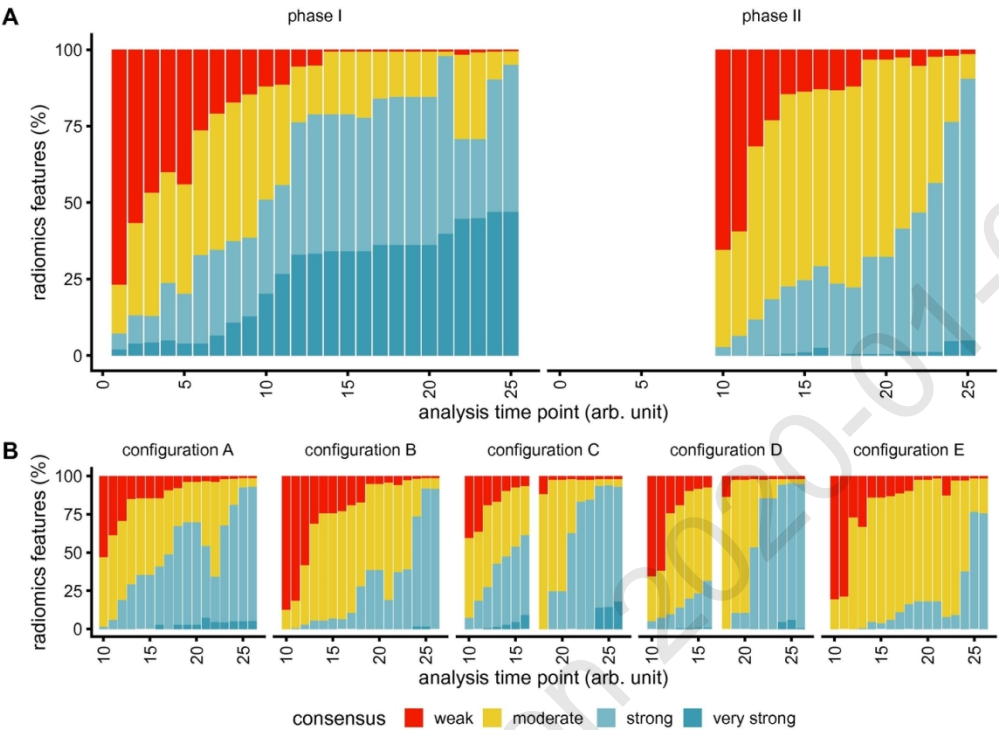


fig 4 Iterative development of consensus on the validity of reference values for radiomics features. We tried to find reliable reference values for radiomics features in an iterative standardization process. In phase I features were computed without prior image processing, whereas in phase II features were assessed after image processing with five predefined configurations (conf. A-E; supplementary note B). The panels show the overall development of consensus on the validity of (tentative) reference values in phases I and II (A) and the development of consensus in phase II, split by image processing configuration (B). Consensus on the validity of a reference value is based on the number of research teams that produce the same value for a feature: weak < 3; moderate: 3-5; strong: 6-9; very strong: ≥ 10 . We analyzed consensus at each of the analysis time points, the time between which was variable (arbitrary unit; arb. unit). New features were included at time points 5 and 22, causing an apparent decrease in consensus. For phase II, we first analyzed consensus at time point 10. Image processing configurations C and D were altered after time point 16. Configuration E was altered after revising the re-segmentation processing step at time point 22. See supplementary note D for more information regarding the timeline.

121x87mm (300 x 300 DPI)

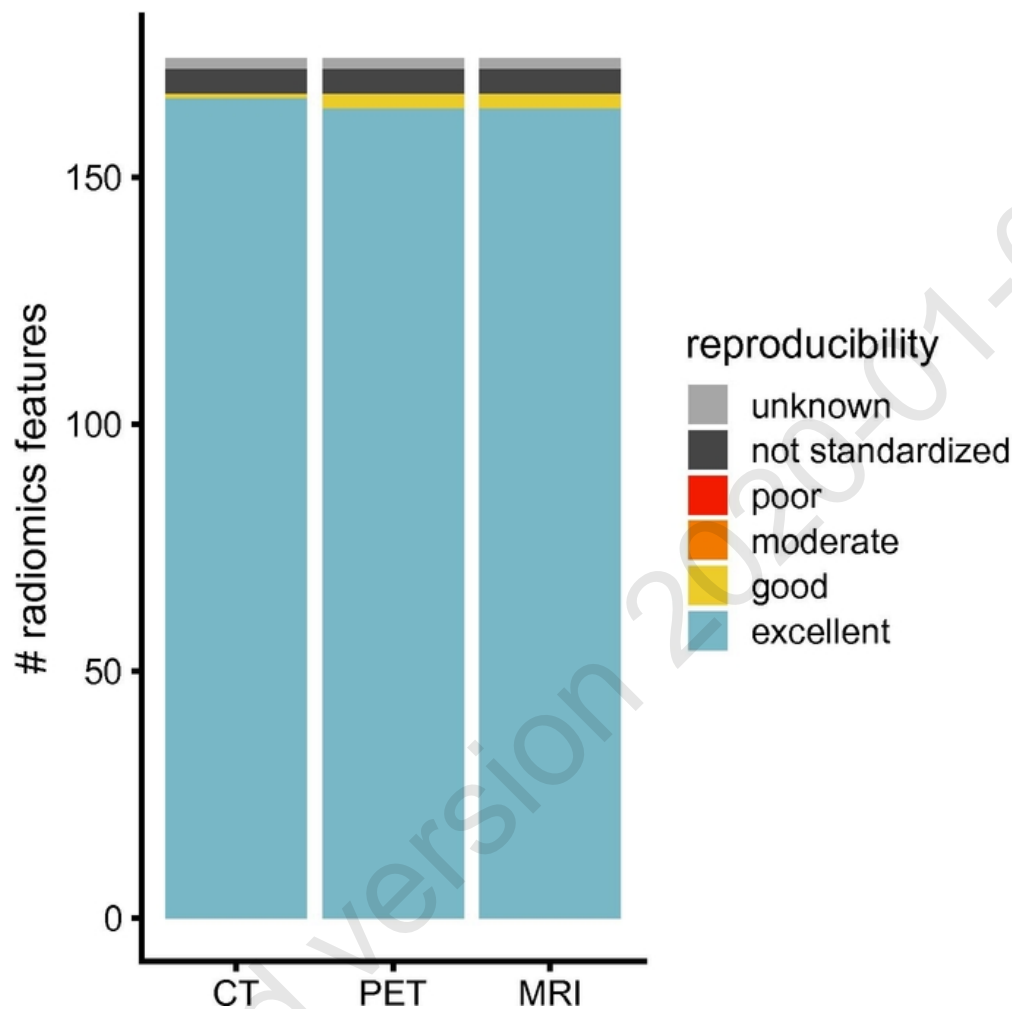


fig 5 Reproducibility of standardized radiomics features. We assessed reproducibility of 169 standardized features on a validation cohort of 51 patients with soft-tissue sarcoma and multi-modality imaging (CT, 18F-FDG-PET, T1-weighted MR; shown as CT, PET and MRI), based on the feature values computed by research teams. We assigned each feature to a reproducibility category based on the lower boundary of the 95% confidence interval of the two-way random effects, single rater, absolute agreement intraclass correlation coefficient of the feature: poor: < 0.50 ; moderate: $0.50-0.75$; good: $0.75-0.90$; excellent: ≥ 0.90 . Five features could not be standardized in this study. Two features with unknown reproducibility were computed by fewer than two teams during validation.

57x57mm (300 x 300 DPI)

1
2
3
4
5
6
7
8
9
10
11
12
13
14
15
16
17
18
19
20
21
22
23
24
25
26
27
28
29
30
31
32
33
34
35
36
37
38
39
40
41
42
43
44
45
46
47
48
49
50
51
52
53
54
55
56
57
58
59
60

The Image Biomarker Standardization Initiative:
standardized quantitative radiomics for high-throughput
image-based phenotyping

Supplementary notes

Accepted version 2020-01-07

Supplementary note A: Features and feature-specific parameters

Some features require specific parameters to compute them, as is detailed in chapter 3 and again summarised in chapter 4 of the IBSI reference manual. In case default parameters exist (e.g. grey level co-occurrence matrix (GLCM) distance equal to 1), these were used. This leaves feature aggregation parameters for all texture features and intensity and volume fraction parameters for intensity-volume histogram (IVH) features.

IVH features were computed at 10% and 90% intensity and volume fractions, leading to a static increase of two features over the number of base definitions found in the reference manual. In the main manuscript, these features are already accounted for.

Texture features are computed from texture matrices. Such matrices may be computed along directions in a grid (2D) or volume (3D), or using 2D or 3D neighborhoods. Grey level co-occurrence and run length matrices (GLRLM) are directional, whereas grey level size zone (GLSZM), distance zone (GLDZM), neighborhood grey tone difference (NGTDM) and neighboring grey level dependence (NGLDM) matrices are based on neighborhoods. Aggregation methods can be specified according to whether matrices are directional or neighborhood.

For directional matrices six different aggregation methods can be designed. Four of these methods pertain to 2D analysis, and the remaining two to 3D analysis. This effectively multiplies the number of texture features by a factor four, two and six for 2D, 3D and combined analyses, respectively.

For neighborhood-based matrices three different aggregation methods can be designed, two of which pertain to 2D analysis and one to 3D analysis. The number of features is then multiplied by a factor of two or three for 2D and combined analyses, respectively.

Supplementary note B: Image processing configurations

Phase I — Finding reference values for radiomics features

In phase I, we attempted to obtain reference values for radiomics features in the absence of image processing. Hence, image processing settings were functionally absent. However, if some standard settings were required to be set, we used the following:

Parameter	Configuration
slice-wise (2D) or single volume (3D)	2D and 3D
interpolation	none
re-segmentation	none
discretisation	none or FBS: 1 or FBN: 6

Table N1: Image processing parameters for the digital phantom used in phase I. The configuration does not alter the image or its mask in any way.

Phase II — Finding reference values for radiomics features using a standardized image processing scheme

In phase II, we attempted to find reference values for radiomics features with image processing, which is a more realistic scenario. We therefore defined the following five configurations that cover several commonly used parameter settings. These configurations do not necessarily represent recommended settings.

Parameter	Config. A	Config. B	Config. C	Config. D	Config. E
slice-wise (2D) or single volume (3D)	2D	2D	3D	3D	3D
interpolation	none	yes	yes	yes	yes
resampled voxel spacing (mm)		2 × 2 (axial)	2 × 2 × 2	2 × 2 × 2	2 × 2 × 2
interpolation method		bilinear	trilinear	trilinear	tricubic spline
intensity rounding		nearest integer	nearest integer	nearest integer	nearest integer
ROI interpolation method		bilinear	trilinear	trilinear	trilinear
ROI partial mask volume		0.5	0.5	0.5	0.5
re-segmentation					
range (HU)	[-500, 400]	[-500, 400]	[-1000, 400]	none	[-1000, 400]
outlier filtering	none	none	none	3σ	3σ
discretisation					
texture and IH	FBS: 25 HU	FBN: 32 bins	FBS: 25 HU	FBN: 32 bins	FBN: 32 bins
IVH	none	none	FBS: 2.5 HU	none	FBN: 1000 bins
texture					
GLCM, NGTDM, NGLDM distance	1	1	1	1	1
GLSZM, GLDZM linkage distance	1	1	1	1	1
NGLDM coarseness	0.0	0.0	0.0	0.0	0.0

Table N2: Image processing parameter configurations for finding reference values for radiomics features using the lung cancer CT image. ROI: region of interest; HU: Hounsfield Unit; IH: intensity histogram; IVH: intensity-volume histogram; FBS: fixed bin size; FBN: fixed bin number; GLCM: grey level co-occurrence matrix; NGTDM: neighborhood grey tone difference matrix; NGLDM: neighbouring grey level dependence matrix; GLSZM: grey level size zone matrix; GLDZM: grey level distance zone matrix.

Phase III — Validation

In phase III, the research teams validated the software implementation of standardized features by assessing reproducibility of standardized radiomics features against a new dataset consisting of CT, 18F-FDG-PET and T1-weighted MR imaging, with a predefined image processing configuration. This dataset was preprocessed to ensure that image processing steps that were not investigated during phase II could not affect reproducibility.

Therefore, prior to validation, PET imaging was converted to body-weight corrected SUV, cropped 50 mm around the GTV ROI and exported to DICOM and NIfTI formats.

T1-weighted MR images were bias-field corrected using the N4 algorithm (1) implemented in ITK 5.0.1, using 3 fitting levels, a maximum of 100 iterations at each level and a convergence threshold of 0.001. Subsequently, the images were normalized on subcutaneous fat intensity to increase comparability between the different MR images, as follows. The 95th percentile of the intensities within the patient mask (i.e. tissue voxels) were used to indicate subcutaneous fat. This was verified for all patients. Afterwards, the image intensities were normalized through linear mapping so that 1000 corresponds to the subcutaneous fat intensity in the original image, and 0 corresponds to 0 in the original image. Next, the images were cropped 50 mm around the GTV ROI. The values in the normalized image were then converted to integers prior to export as DICOM and NIfTI formats.

CT images did not undergo any pre-processing and were exported directly to DICOM and NIfTI formats after cropping to 50 mm around the GTV ROI.

The exported datasets were then shared with the research teams, who extracted feature values according to a modality-specific configuration. These configurations are shown below. Note that these configurations are not necessarily recommended, but are well-adjusted to the available imaging data.

Parameter	CT configuration	PET configuration	MR configuration
slice-wise (2D) or single volume (3D)	3D	3D	3D
interpolation	yes	yes	yes
resampled voxel spacing (mm)	1 × 1 × 1	3 × 3 × 3	1 × 1 × 1
interpolation method	tricubic spline	tricubic spline	tricubic spline
intensity rounding	nearest integer ^a		
ROI interpolation method	trilinear	trilinear	trilinear
ROI partial mask volume	0.5	0.5	0.5
re-segmentation			
range (HU)	[-200, 200]	[0, ∞) ^b	[0, ∞) ^b
outlier filtering	none	none	none
discretisation			
texture and IH	FBS: 10 HU	FBS: 0.25 SUV	FBS: 0.05
IVH	none ^a	FBS: 0.10 SUV	FBS: 0.01
texture ^c			
GLCM, GLRLM aggregation	3D with averaging	3D with averaging	3D with averaging
GLSZM, GLDZM, NGTDM, NGLDM	3D	3D	3D
aggregation			
GLCM, NGTDM, NGLDM distance	1	1	1
GLSZM, GLDZM linkage distance	1	1	1
NGLDM coarseness	0.0	0.0	0.0

Table N3 Image processing parameter configurations for the validation data sets. ROI: region of interest; HU: Hounsfield Unit; SUV: standardized uptake volume. IH: intensity histogram; IVH: intensity-volume histogram; FBS: fixed bin size; FBN: fixed bin number; GLCM: grey level co-occurrence matrix; NGTDM: neighborhood grey tone difference matrix; NGLDM: neighbouring grey level dependence matrix; GLSZM: grey level size zone matrix; GLDZM: grey level distance zone matrix.

^a Default settings.

^b Actual resegmentation is not required. All intensity values fall within this range.

^c No distance weighting is performed. The default distance norms are used.

Supplementary note C: Tolerance margins

Different algorithm choices, rounding errors and other issues may lead to minor deviations from the reference value of radiomics features. These do not constitute errors or lack of compliance, but should be accounted for regardless. Different features display varying sensitivity to minor perturbations. Some, such as the *mean intensity* are relatively stable, but others may vary to a greater extent.

Tolerance was determined for the morphological features in phase I and for all features in phase II. In phase I, tolerance was required since different volume meshing algorithms were found to produce slightly different meshes. Differences in meshes lead to deviations in volume and surface area which are propagated into other morphological features. A narrow tolerance of 0.5% of the reference value was used. For other features no tolerance margin was allowed, as these followed mathematically exact definitions.

In phase II, image processing may lead to minor deviations in feature values. As the response of radiomics features to such perturbations varies and cannot be easily translated into a relative tolerance, we perturbed the image and region of interest mask prior to the interpolation step by rotation and translation in the *xy*-plane with growth and shrinkage of the region of interest (2):

- Rotation: from -15° to 15° in 5° steps.
- Translation: permutations of 0.0, 0.25, 0.50 and 0.75 times the voxel spacing in the *xy*-plane.
- Growth and shrinkage: 2 mm growth, original size and 2 mm shrinkage.

Thus 336 values were produced for each feature using the MIRP software (3). The tolerance margin is then set to 5% of the interquartile range.

A separate spreadsheet is appended to the main manuscript. This file contains the reference values and the tolerance margins of all radiomics features obtained from the digital phantom and those obtained from the lung cancer CT image under five image processing configurations.

Supplementary note D: Study timeline

The first IBSI installment spans the period from June 2016 to October 2019. An overview of the project timeline is provided in Table N4 below.

Date	Time	Description
8 June 2016	—	A draft study proposal was formulated and shared with initial participants.
30 June 2016	—	Final study proposal was formulated and shared. The digital phantom was created and shared, together with the first version of the work document. Phase I was initiated.
14 September 2016	1	Initial contributions for the digital phantom are shared.
9 October 2016	2	Contributions were updated and shared.
24 October 2016	3	The IBSI was presented at the Radiomics meeting in Clearwater, Florida, USA. Contributions were updated and shared.
6 December 2016	4	Contributions were updated and shared.
8 December 2016	—	A major update to the work document was shared with the research teams. Several new features were added, based on requests. <i>Volume</i> and <i>surface area</i> features were re-defined based on meshing algorithms. The general radiomics image processing scheme was drafted.
23 December 2016	5	Contributions were updated and shared. Sections of the work document were posted to <i>arXiv</i> to provide a reference for radiomics features. The dataset for phase II was identified.
24 January 2017	6	Contributions were updated and shared.
30 January 2017	—	The image processing configurations were defined. Phase II was initiated.
10 February 2017	7	Contributions were updated and shared.
24 February 2017	8	Contributions were updated and shared.
10 March 2017	9	Contributions were updated and shared.
14 April 2017	10	Contributions were updated and shared, including initial results for phase II.
21 April 17	—	Segmentation of the RT structure set and image interpolation were identified as major sources of divergence.
6 May 2017	—	Meeting of several IBSI teams during the ESTRO 36 conference, where an electronic poster for IBSI was presented.
19 May 2017	11	Contributions were updated and shared. The description of interpolation is made more precise, and the concept of morphological and intensity ROI masks was introduced.
26 June 2017	12	Contributions were updated and shared.
24 July 2017	13	Contributions were updated and shared. The <i>arXiv</i> document was updated with a new image processing section.
11 August 2017	14	Contributions were updated and shared.
31 August 2017	15	Contributions were updated and shared.
11 October 2017	16	Contributions were updated and shared. First use of tolerance in determining reference values.
23 October 2017	—	Progress of IBSI was presented at the Radiomics meeting in Clearwater, Florida, USA.
16 November 2017	17	Contributions were updated and shared. The <i>arXiv</i> document was updated with a guidelines section, as well as all prior changes to sections of the IBSI work document included in the <i>arXiv</i> document. Configurations C and D were revised. Moreover, the section describing the <i>Intensity-Volume Histogram</i> was extensively revised.
4 December 2017	18	Contributions were updated and shared.
5 January 2018	19	Contributions were updated and shared.
17 January 2018	—	A draft version of the manuscript was prepared and shared with several co-authors.
1 February 2018	—	A revised version of the manuscript was shared with all co-authors.
13 February 2018	20	Late contributions were updated and shared.
20 February 2018	—	Manuscript was sent out for peer-review.
22 August 2018	—	Manuscript was returned with reviewer comments.
30 August 2018	—	Discretisation definitions were updated.
1 October 2018	21	Contributions were updated and shared. The <i>arXiv</i> document was updated to include the improvements to discretisation.
5 October 2018	—	Configuration E was updated to reflect new re-segmentation definitions. 2.5D texture features were added.
16 October 2018	—	Progress of IBSI was presented at the Radiomics meeting in Clearwater, Florida, USA.
22 November 2018	22	Contributions were updated and shared.
4 January 2019	23	Contributions were updated and shared.
1 February 2019	24	Contributions were updated.
1 March 2019	25	Contributions were updated and shared. Consensus on the validity of reference values was

		found to be sufficient to halt the iterative standardization process.
4 April 2019	—	A completely revised version of the manuscript was shared with all co-authors.
16 May 2019	—	The <i>arXiv</i> document was updated to include tables of reference values.
23 May 2019	—	Manuscript was sent out for peer-review.
6 August 2019	—	Review comments were received.
4 September 2019	—	The validation phase (III) was started using new datasets deriving from CT, PET and MR imaging.
14 October 2019	—	All validation results were collected and parsed.
22 October 2019	—	The revised manuscript was submitted for peer-review.
9 December 2019	—	A second revision was submitted.

Table N1: Overview of the project timeline with main events. The time points may be found in figures and tables in this study.

Supplementary note E: Research team information

In total, 25 research teams voluntarily participated in the IBSI. Details are found in Table N5 below. Participation criteria were as follows:

- A team developed their own software for image processing and feature computation.
- A team would participate in at least one phase of the study.

The initial set of teams was invited directly as they were either present at the ESTRO radiomics workshop in 2016, were known to be interested, or had done some early work in the direction of standardization. Teams then also referred to other potentially interested teams of researchers, who then joined as well. Beyond the initial set, most teams joined after learning of the IBSI at conferences or workshops, through colleagues, or after encountering the arXiv preprint. Several open-source developers were directly invited (e.g. LifeX). Recruitment was open at any point during the study.

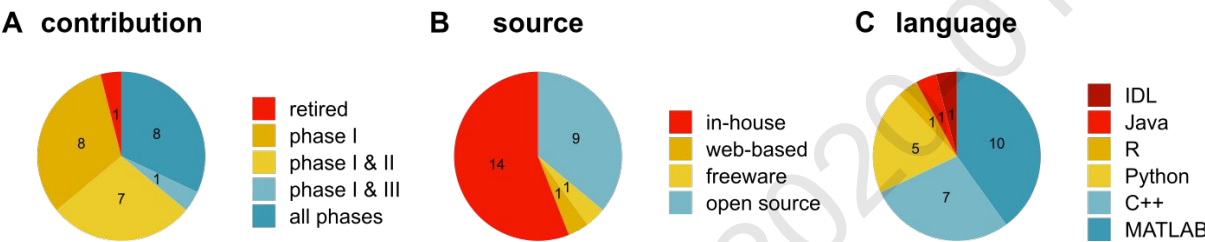


Figure N1: Details concerning the teams and their software implementations. (A) Graph showing the number of teams involved in each phase. One team retired because they switched to software developed by another team. (B) Source code and software availability, and (C) the main programming languages of the research teams..

As shown in Figure N1, eleven of the twenty-five teams developed publicly available software implementations: McGill (4–6), MITK (7), Pyradiomics (8), CERR (9), QuantImage (10), QIFE (11), RaCaT (12), CaPTk (13,14), LIFEx (15), SERA (16) and MIRP (3). The remainder used in-house software.

Team	Institution	Main developer	First entry	Language	Availability
Brest (BCOM)	INSERM Brest	Taman Upadhaya	1	C++	in-house
Brest (MaCha)	INSERM Brest	Marie-Charlotte Desseroit, Baptiste Laurent	1	C++	in-house
Gemelli	Fondazione Policlinico Universitario Agostino Gemelli	Jacopo Lenkowicz	1	R	in-house
LUMC	Leiden University Medical Center (LUMC), VU University Medical Center	Floris H.P. van Velden, Ronald Boellaard	1	IDL	in-house
McGill	McGill University	Martin Vallières	1	MATLAB	open source ¹
MITK	German Cancer Research Center (DKFZ)	Michael Götz, Fabian Isensee, Jonas Scherer	1	C++	open source ²
Moffitt	Moffitt Cancer Center	Mahmoud A. Abdalah	1	C++	in-house
NKI ³	the Netherlands Cancer Institute (NKI)	Cuong Viet Dinh	1	C++	in-house
MIRP	OncoRay – National Center for Radiation Research in Oncology	Alex Zwanenburg, Stefan Leger	1	Python	open source ³
Tuebingen	University of Tübingen		1	Python	in-house

¹ <https://github.com/mvallieres/radiomics-develop>

² <http://mitk.org>

³ <https://github.com/oncoray/mirp>

UMCG (van Dijk)	University Medical Center Groningen (UMCG)	Lisanne V. van Dijk	1	MATLAB	in-house
USZ	University of Zurich	Marta Bogowicz	1	Python	in-house
MAASTRO	Maastricht University Medical Centre+	Ralph T.H. Leijenaar	2	MATLAB	in-house
Cardiff	Cardiff University	Philip Whybra	4	MATLAB	in-house
UMCG (Beukinga)	University Medical Center Groningen (UMCG)	Roelof J. Beukinga	8	MATLAB	in-house
Pyradiomics	the Netherlands Cancer Institute (NKI), Maastricht University, Dana-Farber Cancer Institute	Joost van Griethuysen, Andriy Fedorov	9	Python	open source ⁴
UCSF	University of California, San Francisco (UCSF)	Olivier Morin	10	Python	in-house
CERR	Memorial Sloan Kettering Cancer Center	Aditya Apte	11	MATLAB	open source ⁵
SERA	Johns Hopkins University	Saeed Ashrafinia	12	MATLAB	open source ⁶
QuantImage	University of Applied Sciences Western Switzerland (HES-SO)	Adrien Depeursinge, Vincent Andrearczyk	18	MATLAB	web-based ⁷
QIFE	Stanford University	Sebastian Echegaray, Sarah Mattonen	20	MATLAB	open source ⁸
RaCaT	University Medical Center Groningen (UMCG)	Elisabeth Pfähler	21	C++	open source ⁹
CaPTk	University of Pennsylvania	Sarthak Pati, Sung Min Ha	21	C++	open source ¹⁰
LIFEx	Université Paris Saclay	Christophe Nioche	21	Java	freeware ¹¹
KCL	King's College London	Muhammad Siddique	22	MATLAB	in-house

Table N5: Details regarding the participating research teams. The institution is the main institution at which the developers worked, which were either universities, university medical centers or research institutions. The main developers were primarily responsible for developing, testing and adapting source code during the course of the project. The first entry is the time point at which the team's contribution was first incorporated.

^a This research team retired after stopping development of their software and switching to the software developed by another participant (pyradiomics).

⁴ <https://github.com/Radiomics/pyradiomics>

⁵ <https://github.com/cerr/CERR>

⁶ <https://github.com/ashrafinia/SERA>

⁷ <https://radiomics.hevs.ch/>

⁸ https://github.com/riipl/3d_qifp

⁹ <https://github.com/ellipfaehlerUMCG/RaCat>

¹⁰ <https://github.com/CBICA/CaPTk>

¹¹ <https://www.lifexsoft.org/>

Supplementary note F: Coverage of features per research team

Research teams were not required to implement every feature and support all image processing options. This led to a feature coverage that varied between teams, which is shown in Figure N2 below. Nine teams implemented >50% of the features, and five teams implemented > 95% of the features.

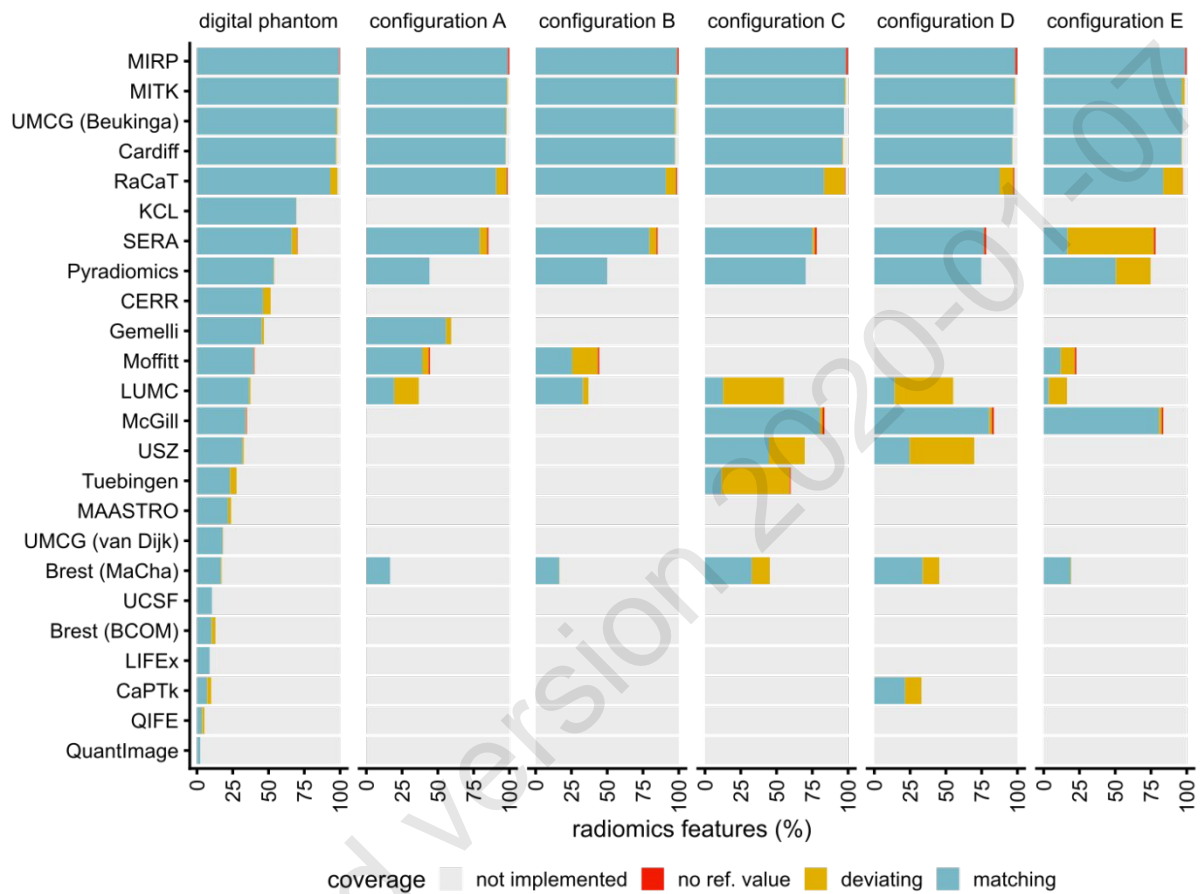


Figure N2: Feature coverage of each research team at the final analysis time point for phases I and II. Features were extracted from the digital phantom (phase I) and from a CT lung cancer image using image processing configurations A-E (phase II). “no ref. value” indicates that there was no consensus on a reference value of a feature, i.e. the number of matching values produced by the teams was < 3, or matching values were produced by ≤50% of contributing teams. “Deviating” indicates that a feature was implemented, but deviated from the reference value. “Matching” indicates that a feature was implemented and the reference value could be reproduced by the team. The number of features is different for each dataset due to different availability of texture matrix aggregation methods: 487 (digital phantom), 351 (configurations A, B), and 215 (configurations C-E).

Supplementary note G: Number of unique institutions and consensus

Research teams that are part of the same institution may potentially share the same code. We did not find any evidence to support this. Four teams shared an institution and developed their software using the same language. Concurrent submissions from these teams showed differences in feature values, which is evidence against using the same code. However, even if the same code was being used by multiple teams within an institution, the effect on consensus is weak, as shown below.

As shown in Table N6 below, the minimum number of unique top-level institutions with matching values was:

- 3 for features with moderate consensus.
- 5 for features with strong consensus.
- 8 for features with very strong consensus.

Note that consensus on the validity of reference values is based on the number of research teams that reproduced the reference value: 3: weak; 3-5: moderate; 6-9: strong; ≥ 10 very strong. Hence the same number of unique top-level institutions may appear for multiple consensus levels.

Consensus level	Unique top-level institutions	Number of features
weak	1	16
weak	2	5
moderate	3	20
moderate	4	56
moderate	5	54
strong	5	224
strong	6	559
strong	7	390
strong	8	199
strong	9	14
very strong	8	2
very strong	9	126
very strong	10	19
very strong	11	27
very strong	12	30
very strong	13	27
very strong	14	30
very strong	15	10
very strong	16	16
very strong	17	2
very strong	18	4
very strong	19	2
very strong	20	2

Table N6: The number of unique top-level institutions for features grouped by the level of consensus on the validity of their reference values.

Supplementary note H: Number of unique programming languages and consensus

Though the research teams developed independent software, the underlying routines may be based on standard implementations. For example, most, if not all, languages have a standard implementation for the *mean* function. Reference values should be based on more than one language to avoid potential reliance on a single standard implementation. As shown in Table N7 below, this is the case for all features with moderate or better consensus.

Note that consensus on the validity of reference values is based on the number of research teams that reproduced the reference value: 3: weak; 3-5: moderate; 6-9: strong; ≥ 10 very strong. Hence the same number of unique programming languages may appear for multiple consensus levels.

Consensus level	Unique languages	Number of features
weak	1	16
weak	2	5
moderate	2	7
moderate	3	123
strong	3	934
strong	4	393
strong	5	59
very strong	3	100
very strong	4	111
very strong	5	81
very strong	6	5

Table N7: The number of unique programming languages for features grouped by the level of consensus on the validity of their reference values.

Supplementary note I: Features with a weak consensus

Moderate or better consensus could not be established for every feature. These features are the same across the different data sets, namely the area and volume densities derived from the minimum volume enclosing ellipsoid (MVEE) and the oriented minimum bounding box (OMBB). OMBB and MVEE both rely on complex algorithmic optimisers that are not commonly implemented. The OMBB for the digital phantom is easily determined, as it is the same as the axis-aligned bounding box.

Data set	Feature	Matches	Dissent
digital phantom	Area density (MVEE)	1	3
digital phantom	Volume density (MVEE)	1	3
configuration A	Area under the IVH curve	3	3
configuration A	Area density (MVEE)	2	1
configuration A	Area density (OMBB)	1	3
configuration A	Volume density (MVEE)	1	2
configuration A	Volume density (OMBB)	1	3
configuration B	Area under the IVH curve	3	3
configuration B	Area density (MVEE)	1	2
configuration B	Area density (OMBB)	1	3
configuration B	Volume density (MVEE)	1	3
configuration B	Volume density (OMBB)	1	3
configuration C	Area density (MVEE)	1	2
configuration C	Area density (OMBB)	1	3
configuration C	Volume density (MVEE)	1	3
configuration C	Volume density (OMBB)	2	2
configuration D	Area density (MVEE)	1	2
configuration D	Area density (OMBB)	2	2
configuration D	Volume density (MVEE)	1	2
configuration D	Volume density (OMBB)	2	2
configuration E	Volume density (MVEE)	1	3
configuration E	Area density (MVEE)	1	4
configuration E	Volume density (OMBB)	2	2

Table N8: Features with a weak level of consensus. These are features describing morphological features based on the oriented minimum bounding box (OMBB) and the minimum volume enclosing ellipsoid (MVEE). The number of matches and the number of dissenting research teams is shown.

Supplementary note J: Detailed information regarding feature implementations

Table N9 below contains information concerning each feature at its initial introduction and after the final iteration:

- The number of research teams that were able to reproduce the tentative reference value of a feature.
- The number of teams that contributed a value.
- The total number of teams.

	First entry			Final entry		
	<i>matching</i>	<i>implem.</i>	<i>total</i>	<i>matching</i>	<i>implem.</i>	<i>total</i>
Morphological features						
Volume (mesh)	8	10	12	11	12	24
Volume (voxel counting)	13	13	17	21	21	24
Surface area (mesh)	1	11	12	11	12	24
Surface to volume ratio	1	11	12	10	12	24
Compactness 1	1	11	12	9	11	24
Compactness 2	1	11	12	9	11	24
Spherical disproportion	1	11	12	9	11	24
Sphericity	1	11	12	10	12	24
Asphericity	0	9	12	8	11	24
Centre of mass shift	7	9	12	15	15	24
Maximum 3D diameter	4	9	12	8	12	24
Major axis length	2	10	12	14	17	24
Minor axis length	2	9	12	11	17	24
Least axis length	2	9	12	11	17	24
Elongation	6	9	12	14	19	24
Flatness	6	9	12	13	18	24
Volume density (AABB)	2	3	14	6	8	24
Area density (AABB)	1	3	14	7	8	24
Volume density (OMBB)	2	2	14	3	3	24
Area density (OMBB)	2	2	14	3	3	24
Volume density (AEE)	2	2	14	5	7	24
Area density (AEE)	2	2	14	5	6	24
Volume density (MVEE)	1	2	14	1	4	24
Area density (MVEE)	1	2	14	1	4	24
Volume density (convex hull)	2	2	14	6	7	24
Area density (convex hull)	2	2	14	7	7	24
Integrated intensity	3	3	14	5	8	24
Moran's I index	2	2	14	7	7	24
Geary's C measure	2	2	14	7	7	24
Local intensity features						
Local intensity peak	1	2	14	8	8	24
Global intensity peak	1	2	14	6	7	24
Intensity-based statistical features						

Mean	12	12	12	23	23	24
Variance	6	12	12	14	22	24
Skewness	10	12	12	21	23	24
(Excess) kurtosis	6	12	12	20	23	24
Median	9	10	12	20	20	24
Minimum	11	11	12	23	23	24
10th percentile	9	9	12	18	18	24
90th percentile	5	9	12	12	18	24
Maximum	11	11	12	22	22	24
Interquartile range	8	9	12	20	20	24
Range	10	10	12	19	19	24
Mean absolute deviation	9	10	12	19	19	24
Robust mean absolute deviation	7	9	12	17	17	24
Median absolute deviation	2	2	14	12	12	24
Coefficient of variation	1	2	14	12	14	24
Quartile coefficient of dispersion	2	2	14	12	12	24
Energy	10	10	12	17	17	24
Root mean square	9	9	12	17	17	24

Intensity histogram features

Mean	4	4	14	13	13	24
Variance	2	4	14	9	12	24
Skewness	4	4	14	12	13	24
Kurtosis	3	4	14	12	13	24
Median	3	4	14	11	11	24
Minimum	4	4	14	13	13	24
10th percentile	4	4	14	10	10	24
90th percentile	3	4	14	7	10	24
Maximum	4	4	14	12	12	24
Mode	2	2	14	10	10	24
Interquartile range	3	4	14	11	11	24
Range	4	4	14	11	11	24
Mean absolute deviation	3	4	14	11	11	24
Robust mean absolute deviation	4	4	14	10	10	24
Median absolute deviation	2	2	14	10	10	24
Coefficient of variation	1	2	14	10	10	24
Quartile coefficient of dispersion	2	2	14	10	10	24
Entropy	8	11	12	19	19	24
Uniformity	8	10	12	19	19	24
Maximum histogram gradient	2	2	14	10	10	24
Maximum histogram gradient intensity	2	2	14	8	10	24
Minimum histogram gradient	2	2	14	10	10	24
Minimum histogram gradient intensity	2	2	14	9	10	24

Intensity-volume histogram features

Volume fraction at 10% intensity	2	2	14	10	10	24
Volume fraction at 90% intensity	2	2	14	10	10	24
Intensity at 10% volume	1	2	14	10	10	24
Intensity at 90% volume	1	2	14	10	10	24
Volume fraction difference between 10% and 90% intensity	2	2	14	10	10	24
Intensity difference between 10% and 90% volume	2	2	14	10	10	24

Area under the IVH curve	1	2	14	8	9	24
Co-occurrence matrix (2D, averaged) features						
Joint maximum	2	3	12	10	10	24
Joint average	1	3	12	10	10	24
Joint variance	1	3	12	10	10	24
Joint entropy	2	3	12	10	10	24
Difference average	1	3	12	10	10	24
Difference variance	1	3	12	10	10	24
Difference entropy	1	3	12	10	10	24
Sum average	2	3	12	10	10	24
Sum variance	1	3	12	10	10	24
Sum entropy	1	3	12	10	10	24
Angular second moment	2	3	12	10	10	24
Contrast	2	3	12	10	10	24
Dissimilarity	2	3	12	10	10	24
Inverse difference	1	2	12	10	10	24
Normalized inverse difference	1	2	12	10	10	24
Inverse difference moment	1	3	12	10	10	24
Normalized inverse difference moment	2	3	12	10	10	24
Inverse variance	1	2	12	10	10	24
Correlation	1	3	12	10	10	24
Autocorrelation	2	3	12	10	10	24
Cluster tendency	2	3	12	10	10	24
Cluster shade	2	3	12	10	10	24
Cluster prominence	2	3	12	10	10	24
Information correlation 1	1	3	12	10	10	24
Information correlation 2	1	3	12	9	10	24
Co-occurrence matrix (2D, slice-merged) features						
Joint maximum	1	1	12	9	9	24
Joint average	1	1	12	9	9	24
Joint variance	1	1	12	9	9	24
Joint entropy	1	1	12	9	9	24
Difference average	1	1	12	9	9	24
Difference variance	1	1	12	9	9	24
Difference entropy	1	1	12	9	9	24
Sum average	1	1	12	9	9	24
Sum variance	1	1	12	9	9	24
Sum entropy	1	1	12	9	9	24
Angular second moment	1	1	12	9	9	24
Contrast	1	1	12	9	9	24
Dissimilarity	1	1	12	9	9	24
Inverse difference	1	1	12	9	9	24
Normalized inverse difference	1	1	12	9	9	24
Inverse difference moment	1	1	12	9	9	24
Normalized inverse difference moment	1	1	12	9	9	24
Inverse variance	1	1	12	9	9	24
Correlation	1	1	12	9	9	24
Autocorrelation	1	1	12	9	9	24
Cluster tendency	1	1	12	9	9	24
Cluster shade	1	1	12	9	9	24

Cluster prominence	1	1	12	9	9	24
Information correlation 1	1	1	12	9	9	24
Information correlation 2	1	1	12	8	9	24

Co-occurrence matrix (2.5D, direction-merged) features

Joint maximum	4	4	21	8	8	24
Joint average	4	4	21	8	8	24
Joint variance	4	4	21	8	8	24
Joint entropy	4	4	21	8	8	24
Difference average	4	4	21	8	8	24
Difference variance	4	4	21	8	8	24
Difference entropy	4	4	21	8	8	24
Sum average	4	4	21	8	8	24
Sum variance	4	4	21	8	8	24
Sum entropy	4	4	21	8	8	24
Angular second moment	4	4	21	8	8	24
Contrast	4	4	21	8	8	24
Dissimilarity	4	4	21	8	8	24
Inverse difference	4	4	21	8	8	24
Normalized inverse difference	4	4	21	8	8	24
Inverse difference moment	4	4	21	8	8	24
Normalized inverse difference moment	4	4	21	8	8	24
Inverse variance	4	4	21	8	8	24
Correlation	4	4	21	8	8	24
Autocorrelation	4	4	21	8	8	24
Cluster tendency	4	4	21	8	8	24
Cluster shade	4	4	21	8	8	24
Cluster prominence	4	4	21	8	8	24
Information correlation 1	4	4	21	8	8	24
Information correlation 2	4	4	21	7	8	24

Co-occurrence matrix (2.5D, merged) features

Joint maximum	4	4	21	8	8	24
Joint average	4	4	21	8	8	24
Joint variance	4	4	21	8	8	24
Joint entropy	4	4	21	8	8	24
Difference average	4	4	21	8	8	24
Difference variance	4	4	21	8	8	24
Difference entropy	4	4	21	8	8	24
Sum average	4	4	21	8	8	24
Sum variance	4	4	21	8	8	24
Sum entropy	4	4	21	8	8	24
Angular second moment	4	4	21	8	8	24
Contrast	4	4	21	8	8	24
Dissimilarity	4	4	21	8	8	24
Inverse difference	4	4	21	8	8	24
Normalized inverse difference	4	4	21	8	8	24
Inverse difference moment	4	4	21	8	8	24
Normalized inverse difference moment	4	4	21	8	8	24
Inverse variance	4	4	21	8	8	24
Correlation	4	4	21	8	8	24
Autocorrelation	4	4	21	8	8	24

Cluster tendency	4	4	21	8	8	24
Cluster shade	4	4	21	8	8	24
Cluster prominence	4	4	21	8	8	24
Information correlation 1	4	4	21	8	8	24
Information correlation 2	4	4	21	7	8	24

Co-occurrence matrix (3D, averaged) features

Joint maximum	2	6	12	15	15	24
Joint average	2	5	12	14	15	24
Joint variance	1	6	12	13	15	24
Joint entropy	3	6	12	17	18	24
Difference average	2	5	12	14	14	24
Difference variance	2	6	12	15	15	24
Difference entropy	3	7	12	15	15	24
Sum average	2	7	12	15	15	24
Sum variance	2	7	12	15	15	24
Sum entropy	4	7	12	15	16	24
Angular second moment	2	8	12	18	18	24
Contrast	2	8	12	18	19	24
Dissimilarity	2	7	12	16	16	24
Inverse difference	1	6	12	16	16	24
Normalized inverse difference	1	6	12	14	14	24
Inverse difference moment	1	8	12	16	16	24
Normalized inverse difference moment	1	6	12	15	15	24
Inverse variance	1	6	12	14	14	24
Correlation	2	7	12	16	19	24
Autocorrelation	2	7	12	14	14	24
Cluster tendency	2	6	12	14	14	24
Cluster shade	2	8	12	16	17	24
Cluster prominence	2	8	12	16	16	24
Information correlation 1	1	7	12	14	14	24
Information correlation 2	1	7	12	14	14	24

Co-occurrence matrix (3D, merged) features

Joint maximum	2	4	12	15	15	24
Joint average	2	4	12	15	15	24
Joint variance	2	4	12	15	15	24
Joint entropy	2	4	12	16	16	24
Difference average	2	4	12	14	15	24
Difference variance	2	4	12	14	15	24
Difference entropy	2	4	12	15	15	24
Sum average	2	4	12	15	15	24
Sum variance	2	4	12	14	15	24
Sum entropy	2	4	12	15	15	24
Angular second moment	2	4	12	16	16	24
Contrast	2	4	12	15	16	24
Dissimilarity	2	4	12	15	15	24
Inverse difference	2	4	12	15	15	24
Normalized inverse difference	2	4	12	15	15	24
Inverse difference moment	2	4	12	16	16	24
Normalized inverse difference moment	2	4	12	15	15	24
Inverse variance	2	4	12	15	15	24

Correlation	2	4	12	15	16	24
Autocorrelation	2	4	12	15	15	24
Cluster tendency	2	4	12	15	15	24
Cluster shade	2	4	12	16	16	24
Cluster prominence	3	4	12	15	16	24
Information correlation 1	2	4	12	14	15	24
Information correlation 2	1	4	12	15	15	24

Run length matrix (2D, averaged) features

Short runs emphasis	1	2	12	10	10	24
Long runs emphasis	1	2	12	10	10	24
Low grey level run emphasis	1	2	12	10	10	24
High grey level run emphasis	1	2	12	10	10	24
Short run low grey level emphasis	1	2	12	10	10	24
Short run high grey level emphasis	1	2	12	10	10	24
Long run low grey level emphasis	1	2	12	10	10	24
Long run high grey level emphasis	1	2	12	10	10	24
Grey level non-uniformity	1	2	12	10	10	24
Normalized grey level non-uniformity	1	1	12	10	10	24
Run length non-uniformity	1	2	12	10	10	24
Normalized run length non-uniformity	1	1	12	10	10	24
Run percentage	1	2	12	10	10	24
Grey level variance	1	2	12	10	10	24
Run length variance	1	2	12	10	10	24
Run entropy	1	2	12	10	10	24

Run length matrix (2D, slice-merged) features

Short runs emphasis	1	1	12	9	9	24
Long runs emphasis	1	1	12	9	9	24
Low grey level run emphasis	1	1	12	9	9	24
High grey level run emphasis	1	1	12	9	9	24
Short run low grey level emphasis	1	1	12	9	9	24
Short run high grey level emphasis	1	1	12	9	9	24
Long run low grey level emphasis	1	1	12	9	9	24
Long run high grey level emphasis	1	1	12	9	9	24
Grey level non-uniformity	1	1	12	9	9	24
Normalized grey level non-uniformity	1	1	12	9	9	24
Run length non-uniformity	1	1	12	9	9	24
Normalized run length non-uniformity	1	1	12	9	9	24
Run percentage	1	1	12	7	9	24
Grey level variance	1	1	12	9	9	24
Run length variance	1	1	12	9	9	24
Run entropy	1	1	12	9	9	24

Run length matrix (2.5D, direction-merged) features

Short runs emphasis	3	4	21	8	8	24
Long runs emphasis	3	4	21	8	8	24
Low grey level run emphasis	3	4	21	8	8	24
High grey level run emphasis	3	4	21	8	8	24
Short run low grey level emphasis	3	4	21	8	8	24
Short run high grey level emphasis	3	4	21	8	8	24
Long run low grey level emphasis	3	4	21	8	8	24

1							
2							
3	Long run high grey level emphasis	3	4	21	8	8	24
4	Grey level non-uniformity	3	4	21	8	8	24
5	Normalized grey level non-uniformity	3	4	21	8	8	24
6	Run length non-uniformity	3	4	21	8	8	24
7	Normalized run length non-uniformity	3	4	21	8	8	24
8	Run percentage	2	4	21	7	8	24
9	Grey level variance	3	4	21	8	8	24
10	Run length variance	3	4	21	8	8	24
11	Run entropy	3	4	21	7	7	24
12							
13							
14	Run length matrix (2.5D, merged) features						
15	Short runs emphasis	3	4	21	8	8	24
16	Long runs emphasis	3	4	21	8	8	24
17	Low grey level run emphasis	3	4	21	8	8	24
18	High grey level run emphasis	3	4	21	8	8	24
19	Short run low grey level emphasis	3	4	21	8	8	24
20	Short run high grey level emphasis	3	4	21	8	8	24
21	Long run low grey level emphasis	3	4	21	8	8	24
22	Long run high grey level emphasis	3	4	21	8	8	24
23	Grey level non-uniformity	3	4	21	8	8	24
24	Normalized grey level non-uniformity	3	4	21	8	8	24
25	Run length non-uniformity	3	4	21	8	8	24
26	Normalized run length non-uniformity	3	4	21	8	8	24
27	Run percentage	3	4	21	6	8	24
28	Grey level variance	2	4	21	7	8	24
29	Run length variance	2	4	21	7	8	24
30	Run entropy	2	4	21	6	7	24
31							
32							
33							
34	Run length matrix (3D, averaged) features						
35	Short runs emphasis	4	8	12	16	17	24
36	Long runs emphasis	4	8	12	15	17	24
37	Low grey level run emphasis	4	8	12	17	18	24
38	High grey level run emphasis	5	8	12	17	18	24
39	Short run low grey level emphasis	2	8	12	15	18	24
40	Short run high grey level emphasis	5	8	12	16	18	24
41	Long run low grey level emphasis	4	8	12	15	18	24
42	Long run high grey level emphasis	4	8	12	15	18	24
43	Grey level non-uniformity	5	8	12	16	17	24
44	Normalized grey level non-uniformity	3	4	12	14	15	24
45	Run length non-uniformity	2	8	12	16	17	24
46	Normalized run length non-uniformity	1	4	12	14	15	24
47	Run percentage	4	7	12	15	16	24
48	Grey level variance	3	5	12	14	15	24
49	Run length variance	2	5	12	14	15	24
50	Run entropy	4	5	12	14	14	24
51							
52							
53							
54	Run length matrix (3D, merged) features						
55	Short runs emphasis	3	4	12	14	14	24
56	Long runs emphasis	3	4	12	13	14	24
57	Low grey level run emphasis	3	4	12	14	14	24
58	High grey level run emphasis	3	4	12	14	14	24
59	Short run low grey level emphasis	3	4	12	13	14	24
60							

Short run high grey level emphasis	3	4	12	14	14	24
Long run low grey level emphasis	3	4	12	13	14	24
Long run high grey level emphasis	4	4	12	13	14	24
Grey level non-uniformity	3	4	12	14	14	24
Normalized grey level non-uniformity	3	3	12	13	13	24
Run length non-uniformity	3	4	12	13	14	24
Normalized run length non-uniformity	3	3	12	13	13	24
Run percentage	3	4	12	12	13	24
Grey level variance	3	4	12	13	13	24
Run length variance	3	4	12	13	13	24
Run entropy	4	4	12	12	12	24

Size zone matrix (2D) features

Small zone emphasis	1	2	12	9	9	24
Large zone emphasis	1	2	12	9	9	24
Low grey level emphasis	1	2	12	9	9	24
High grey level emphasis	1	2	12	9	9	24
Small zone low grey level emphasis	1	2	12	9	9	24
Small zone high grey level emphasis	1	2	12	9	9	24
Large zone low grey level emphasis	1	2	12	9	9	24
Large zone high grey level emphasis	1	2	12	9	9	24
Grey level non-uniformity	2	2	12	9	9	24
Normalized grey level non-uniformity	1	1	12	9	9	24
Zone size non-uniformity	2	2	12	9	9	24
Normalized zone size non-uniformity	1	1	12	9	9	24
Zone percentage	1	2	12	9	9	24
Grey level variance	1	2	12	9	9	24
Zone size variance	1	2	12	9	9	24
Zone size entropy	2	2	12	9	9	24

Size zone matrix (2.5D) features

Small zone emphasis	4	4	21	8	8	24
Large zone emphasis	4	4	21	8	8	24
Low grey level emphasis	4	4	21	8	8	24
High grey level emphasis	4	4	21	8	8	24
Small zone low grey level emphasis	4	4	21	8	8	24
Small zone high grey level emphasis	4	4	21	8	8	24
Large zone low grey level emphasis	4	4	21	8	8	24
Large zone high grey level emphasis	4	4	21	8	8	24
Grey level non-uniformity	4	4	21	8	8	24
Normalized grey level non-uniformity	4	4	21	8	8	24
Zone size non-uniformity	4	4	21	8	8	24
Normalized zone size non-uniformity	4	4	21	8	8	24
Zone percentage	3	4	21	8	8	24
Grey level variance	4	4	21	8	8	24
Zone size variance	4	4	21	8	8	24
Zone size entropy	4	4	21	7	7	24

Size zone matrix (3D) features

Small zone emphasis	5	9	12	19	19	24
Large zone emphasis	6	9	12	19	19	24
Low grey level emphasis	4	9	12	19	19	24

High grey level emphasis	5	9	12	19	19	24
Small zone low grey level emphasis	3	9	12	19	19	24
Small zone high grey level emphasis	5	9	12	19	19	24
Large zone low grey level emphasis	5	9	12	19	19	24
Large zone high grey level emphasis	5	9	12	17	19	24
Grey level non-uniformity	4	9	12	19	19	24
Normalized grey level non-uniformity	4	6	12	17	17	24
Zone size non-uniformity	6	9	12	19	19	24
Normalized zone size non-uniformity	4	6	12	17	17	24
Zone percentage	4	9	12	19	19	24
Grey level variance	5	7	12	17	17	24
Zone size variance	5	7	12	17	17	24
Zone size entropy	5	7	12	16	16	24

Distance zone matrix (2D) features

Small distance emphasis	1	1	12	7	7	24
Large distance emphasis	1	1	12	7	7	24
Low grey level emphasis	1	1	12	7	7	24
High grey level emphasis	1	1	12	7	7	24
Small distance low grey level emphasis	1	1	12	7	7	24
Small distance high grey level emphasis	1	1	12	7	7	24
Large distance low grey level emphasis	1	1	12	7	7	24
Large distance high grey level emphasis	1	1	12	7	7	24
Grey level non-uniformity	1	1	12	7	7	24
Normalized grey level non-uniformity	1	1	12	7	7	24
Zone distance non-uniformity	1	1	12	7	7	24
Normalized zone distance non-uniformity	1	1	12	7	7	24
Zone percentage	1	1	12	7	7	24
Grey level variance	1	1	12	6	7	24
Zone distance variance	1	1	12	7	7	24
Zone distance entropy	1	1	12	7	7	24

Distance zone matrix (2.5D) features

Small distance emphasis	3	3	21	5	5	24
Large distance emphasis	3	3	21	5	5	24
Low grey level emphasis	3	3	21	5	5	24
High grey level emphasis	3	3	21	5	5	24
Small distance low grey level emphasis	3	3	21	5	5	24
Small distance high grey level emphasis	3	3	21	5	5	24
Large distance low grey level emphasis	3	3	21	5	5	24
Large distance high grey level emphasis	3	3	21	5	5	24
Grey level non-uniformity	3	3	21	5	5	24
Normalized grey level non-uniformity	3	3	21	5	5	24
Zone distance non-uniformity	3	3	21	5	5	24
Normalized zone distance non-uniformity	3	3	21	5	5	24
Zone percentage	2	3	21	3	5	24
Grey level variance	3	3	21	5	5	24
Zone distance variance	3	3	21	5	5	24
Zone distance entropy	3	3	21	5	5	24

Distance zone matrix (3D) features

Small distance emphasis	1	2	12	10	11	24
-------------------------	---	---	----	----	----	----

Large distance emphasis	1	2	12	10	11	24
Low grey level emphasis	1	2	12	11	11	24
High grey level emphasis	1	2	12	11	11	24
Small distance low grey level emphasis	1	2	12	10	11	24
Small distance high grey level emphasis	1	2	12	10	11	24
Large distance low grey level emphasis	1	2	12	10	11	24
Large distance high grey level emphasis	1	2	12	10	11	24
Grey level non-uniformity	2	2	12	11	11	24
Normalized grey level non-uniformity	2	2	12	11	11	24
Zone distance non-uniformity	1	2	12	10	11	24
Normalized zone distance non-uniformity	1	2	12	10	11	24
Zone percentage	1	1	12	10	11	24
Grey level variance	2	2	12	11	11	24
Zone distance variance	1	2	12	10	11	24
Zone distance entropy	2	2	12	11	11	24

Neighborhood grey tone difference matrix (2D) features

Coarseness	1	2	12	8	8	24
Contrast	1	2	12	8	8	24
Busyness	1	2	12	8	8	24
Complexity	1	2	12	8	8	24
Strength	1	2	12	8	8	24

Neighborhood grey tone difference matrix (2.5D) features

Coarseness	3	4	21	7	7	24
Contrast	3	4	21	7	7	24
Busyness	3	4	21	6	7	24
Complexity	4	4	21	6	7	24
Strength	3	4	21	6	7	24

Neighborhood grey tone difference matrix (3D) features

Coarseness	2	7	12	18	18	24
Contrast	2	7	12	17	18	24
Busyness	2	7	12	16	18	24
Complexity	2	7	12	14	17	24
Strength	2	7	12	14	17	24

Neighboring grey level dependence matrix (2D) features

Low dependence emphasis	1	1	12	7	7	24
High dependence emphasis	1	1	12	7	7	24
Low grey level count emphasis	1	1	12	7	7	24
High grey level count emphasis	1	1	12	7	7	24
Low dependence low grey level emphasis	1	1	12	7	7	24
Low dependence high grey level emphasis	1	1	12	7	7	24
High dependence low grey level emphasis	1	1	12	7	7	24
High dependence high grey level emphasis	1	1	12	7	7	24
Grey level non-uniformity	1	1	12	7	7	24
Normalized grey level non-uniformity	1	1	12	7	7	24
Dependence count non-uniformity	1	1	12	7	7	24
Normalized dependence count non-uniformity	1	1	12	7	7	24
Dependence count percentage	1	1	12	6	6	24
Grey level variance	1	1	12	7	7	24

Dependence count variance	1	1	12	7	7	24
Dependence count entropy	1	1	12	7	7	24
Dependence count energy	1	1	14	7	7	24

Neighboring grey level dependence matrix (2.5D) features

Low dependence emphasis	4	4	21	7	7	24
High dependence emphasis	4	4	21	7	7	24
Low grey level count emphasis	4	4	21	7	7	24
High grey level count emphasis	4	4	21	7	7	24
Low dependence low grey level emphasis	4	4	21	7	7	24
Low dependence high grey level emphasis	4	4	21	7	7	24
High dependence low grey level emphasis	4	4	21	7	7	24
High dependence high grey level emphasis	4	4	21	7	7	24
Grey level non-uniformity	4	4	21	7	7	24
Normalized grey level non-uniformity	4	4	21	7	7	24
Dependence count non-uniformity	4	4	21	7	7	24
Normalized dependence count non-uniformity	4	4	21	7	7	24
Dependence count percentage	2	2	21	4	5	24
Grey level variance	4	4	21	7	7	24
Dependence count variance	4	4	21	7	7	24
Dependence count entropy	4	4	21	7	7	24
Dependence count energy	3	3	21	6	6	24

Neighboring grey level dependence matrix (3D) features

Low dependence emphasis	1	2	12	12	12	24
High dependence emphasis	1	2	12	12	12	24
Low grey level count emphasis	1	2	12	12	12	24
High grey level count emphasis	1	2	12	12	12	24
Low dependence low grey level emphasis	1	2	12	12	12	24
Low dependence high grey level emphasis	1	2	12	12	12	24
High dependence low grey level emphasis	1	2	12	12	12	24
High dependence high grey level emphasis	1	2	12	12	12	24
Grey level non-uniformity	2	2	12	12	12	24
Normalized grey level non-uniformity	2	2	12	12	12	24
Dependence count non-uniformity	1	2	12	12	12	24
Normalized dependence count non-uniformity	1	2	12	12	12	24
Dependence count percentage	1	1	12	7	7	24
Grey level variance	1	2	12	12	12	24
Dependence count variance	1	2	12	12	12	24
Dependence count entropy	1	2	12	12	12	24
Dependence count energy	2	3	14	10	10	24

Table N9: Details regarding the number of radiomic feature implementations and consensus on the validity of tentative reference values at the initial and final time points for the digital phantom in phase I. Note that while at the final time point the number of research teams is the same for every feature, this is not the case at the initial time point as some radiomics features were introduced later during the iterative process.

Supplementary note K: Feature reproducibility in the validation cohort

For validation, research teams extracted features from CT, 18F-FDG-PET and T1-weighted MR images of 51 patients according to the configurations in supplementary note B. Standardization of each feature by a team was first assessed by determining whether the team could demonstrate that they were able to reproduce the respective reference values under configurations C, D and E (established in phase II). If this was the case, the standardized feature was then used to compute a two-way random effects, single rater, absolute agreement intraclass correlation coefficient (ICC). These ICC values and their 95% confidence intervals are shown in Table N10 below.

	CT	PET	MRI
Morphological features			
Volume (mesh)	0.976 [0.964, 0.985]	0.976 [0.964, 0.985]	0.968 [0.952, 0.980]
Volume (voxel counting)	1.000 [1.000, 1.000]	1.000 [1.000, 1.000]	0.999 [0.999, 1.000]
Surface area (mesh)	1.000 [1.000, 1.000]	1.000 [1.000, 1.000]	0.999 [0.999, 0.999]
Surface to volume ratio	1.000 [1.000, 1.000]	1.000 [1.000, 1.000]	0.999 [0.999, 1.000]
Compactness 1	1.000 [1.000, 1.000]	1.000 [0.999, 1.000]	0.995 [0.993, 0.997]
Compactness 2	1.000 [0.999, 1.000]	0.999 [0.999, 1.000]	0.994 [0.990, 0.996]
Spherical disproportion	1.000 [1.000, 1.000]	1.000 [0.999, 1.000]	0.995 [0.993, 0.997]
Sphericity	1.000 [1.000, 1.000]	1.000 [0.999, 1.000]	0.995 [0.992, 0.997]
Asphericity	1.000 [1.000, 1.000]	0.999 [0.999, 1.000]	0.995 [0.992, 0.997]
Centre of mass shift	1.000 [1.000, 1.000]	0.999 [0.998, 0.999]	0.989 [0.984, 0.993]
Maximum 3D diameter	0.997 [0.996, 0.998]	0.997 [0.995, 0.998]	0.990 [0.984, 0.994]
Major axis length	1.000 [1.000, 1.000]	0.999 [0.999, 1.000]	0.993 [0.990, 0.996]
Minor axis length	1.000 [0.999, 1.000]	0.999 [0.999, 1.000]	0.997 [0.996, 0.998]
Least axis length	1.000 [1.000, 1.000]	1.000 [1.000, 1.000]	1.000 [1.000, 1.000]
Elongation	0.999 [0.999, 1.000]	0.999 [0.998, 0.999]	0.995 [0.993, 0.997]
Flatness	1.000 [0.999, 1.000]	0.999 [0.999, 1.000]	0.992 [0.988, 0.995]
Volume density (AABB)	0.999 [0.998, 0.999]	0.989 [0.984, 0.993]	0.973 [0.959, 0.983]
Area density (AABB)	0.998 [0.997, 0.999]	0.989 [0.983, 0.993]	0.974 [0.961, 0.984]
Volume density (OMBB)	NS	NS	NS
Area density (OMBB)	NS	NS	NS
Volume density (AEE)	1.000 [1.000, 1.000]	1.000 [0.999, 1.000]	1.000 [1.000, 1.000]
Area density (AEE)	1.000 [1.000, 1.000]	0.999 [0.999, 0.999]	1.000 [1.000, 1.000]
Volume density (MVEE)	NS	NS	NS
Area density (MVEE)	NS	NS	NS
Volume density (convex hull)	1.000 [1.000, 1.000]	1.000 [1.000, 1.000]	1.000 [1.000, 1.000]
Area density (convex hull)	1.000 [1.000, 1.000]	1.000 [0.999, 1.000]	1.000 [1.000, 1.000]
Integrated intensity	0.942 [0.915, 0.963]	0.987 [0.980, 0.992]	0.981 [0.971, 0.988]
Moran's I index	NA	NA	NA
Geary's C measure	NA	NA	NA
Local intensity features			
Local intensity peak	1.000 [1.000, 1.000]	0.967 [0.949, 0.980]	0.971 [0.955, 0.982]
Global intensity peak	1.000 [1.000, 1.000]	0.999 [0.999, 1.000]	1.000 [1.000, 1.000]
Intensity-based statistics features			
Mean	0.999 [0.999, 1.000]	0.999 [0.999, 1.000]	0.997 [0.995, 0.998]
Variance	1.000 [1.000, 1.000]	0.999 [0.999, 1.000]	0.997 [0.995, 0.998]
Skewness	1.000 [1.000, 1.000]	0.997 [0.996, 0.998]	0.992 [0.988, 0.995]
(Excess) kurtosis	0.994 [0.992, 0.996]	0.997 [0.996, 0.998]	0.990 [0.986, 0.994]

Median	0.998 [0.998, 0.999]	0.999 [0.999, 1.000]	0.997 [0.995, 0.998]
Minimum	0.990 [0.985, 0.994]	0.972 [0.958, 0.982]	0.983 [0.975, 0.989]
10th percentile	1.000 [1.000, 1.000]	0.999 [0.998, 0.999]	0.997 [0.996, 0.998]
90th percentile	0.999 [0.999, 1.000]	0.999 [0.999, 1.000]	0.998 [0.997, 0.999]
Maximum	0.998 [0.997, 0.999]	0.991 [0.986, 0.994]	0.993 [0.990, 0.996]
Interquartile range	0.999 [0.999, 0.999]	0.999 [0.999, 0.999]	0.996 [0.994, 0.997]
Range	0.994 [0.990, 0.996]	0.990 [0.986, 0.994]	0.990 [0.985, 0.994]
Mean absolute deviation	1.000 [1.000, 1.000]	0.999 [0.999, 1.000]	0.996 [0.994, 0.998]
Robust mean absolute deviation	1.000 [0.999, 1.000]	0.928 [0.895, 0.954]	0.995 [0.993, 0.997]
Median absolute deviation	1.000 [1.000, 1.000]	0.999 [0.999, 1.000]	0.996 [0.994, 0.998]
Coefficient of variation	1.000 [1.000, 1.000]	1.000 [0.999, 1.000]	0.997 [0.995, 0.998]
Quartile coefficient of dispersion	1.000 [1.000, 1.000]	0.998 [0.997, 0.999]	0.998 [0.997, 0.999]
Energy	1.000 [1.000, 1.000]	1.000 [1.000, 1.000]	1.000 [1.000, 1.000]
Root mean square	0.999 [0.998, 0.999]	0.999 [0.999, 0.999]	0.997 [0.995, 0.998]

Intensity histogram features

Mean	1.000 [0.999, 1.000]	0.999 [0.999, 1.000]	0.997 [0.995, 0.998]
Variance	1.000 [1.000, 1.000]	0.999 [0.999, 1.000]	0.997 [0.995, 0.998]
Skewness	1.000 [1.000, 1.000]	0.999 [0.999, 0.999]	0.998 [0.997, 0.999]
(Excess) kurtosis	1.000 [1.000, 1.000]	0.998 [0.997, 0.999]	0.998 [0.997, 0.999]
Median	1.000 [0.999, 1.000]	0.999 [0.999, 0.999]	0.997 [0.996, 0.998]
Minimum	0.992 [0.989, 0.995]	0.940 [0.912, 0.962]	0.984 [0.977, 0.990]
10th percentile	1.000 [1.000, 1.000]	0.996 [0.993, 0.997]	0.997 [0.995, 0.998]
90th percentile	0.977 [0.965, 0.985]	0.998 [0.996, 0.998]	0.993 [0.990, 0.996]
Maximum	0.996 [0.995, 0.998]	0.989 [0.984, 0.993]	0.993 [0.990, 0.996]
Mode	1.000 [1.000, 1.000]	1.000 [0.999, 1.000]	1.000 [0.999, 1.000]
Interquartile range	1.000 [1.000, 1.000]	0.997 [0.996, 0.998]	0.982 [0.973, 0.989]
Range	0.994 [0.991, 0.996]	0.990 [0.984, 0.993]	0.990 [0.985, 0.994]
Mean absolute deviation	1.000 [1.000, 1.000]	0.999 [0.999, 1.000]	0.996 [0.994, 0.998]
Robust mean absolute deviation	1.000 [1.000, 1.000]	1.000 [0.999, 1.000]	0.996 [0.993, 0.997]
Median absolute deviation	1.000 [1.000, 1.000]	0.999 [0.999, 1.000]	0.996 [0.995, 0.998]
Coefficient of variation	1.000 [1.000, 1.000]	1.000 [0.999, 1.000]	0.997 [0.995, 0.998]
Quartile coefficient of dispersion	1.000 [1.000, 1.000]	0.981 [0.971, 0.988]	0.993 [0.990, 0.996]
Entropy	1.000 [1.000, 1.000]	0.999 [0.999, 1.000]	0.995 [0.993, 0.997]
Uniformity	1.000 [1.000, 1.000]	1.000 [0.999, 1.000]	0.996 [0.994, 0.997]
Maximum histogram gradient	1.000 [1.000, 1.000]	0.987 [0.981, 0.992]	0.999 [0.998, 0.999]
Maximum histogram gradient intensity	0.999 [0.999, 1.000]	0.897 [0.847, 0.934]	0.999 [0.999, 1.000]
Minimum histogram gradient	1.000 [1.000, 1.000]	0.992 [0.987, 0.995]	0.999 [0.999, 0.999]
Minimum histogram gradient intensity	0.999 [0.999, 0.999]	1.000 [1.000, 1.000]	0.999 [0.998, 0.999]

Intensity-volume histogram features

Volume fraction at 10% intensity	1.000 [1.000, 1.000]	0.989 [0.983, 0.994]	1.000 [1.000, 1.000]
Volume fraction at 90% intensity	0.882 [0.829, 0.923]	0.830 [0.760, 0.889]	0.872 [0.816, 0.917]
Intensity at 10% volume	0.999 [0.999, 1.000]	0.999 [0.999, 0.999]	0.998 [0.997, 0.999]
Intensity at 90% volume	1.000 [1.000, 1.000]	0.995 [0.992, 0.997]	1.000 [1.000, 1.000]
Volume fraction difference between 10% and 90% intensity	1.000 [1.000, 1.000]	0.985 [0.978, 0.991]	1.000 [1.000, 1.000]
Intensity difference between 10% and 90% volume	1.000 [1.000, 1.000]	0.998 [0.997, 0.999]	0.997 [0.996, 0.998]
Area under the IVH curve	NS	NS	NS

Co-occurrence matrix features

Joint maximum	1.000 [1.000, 1.000]	0.999 [0.999, 1.000]	0.997 [0.996, 0.998]
Joint average	0.999 [0.999, 1.000]	0.999 [0.999, 1.000]	0.997 [0.995, 0.998]

Joint variance	1.000 [1.000, 1.000]	0.999 [0.999, 1.000]	0.996 [0.995, 0.998]
Joint entropy	1.000 [1.000, 1.000]	0.999 [0.999, 1.000]	0.996 [0.994, 0.997]
Difference average	1.000 [1.000, 1.000]	0.999 [0.999, 0.999]	0.996 [0.995, 0.998]
Difference variance	1.000 [1.000, 1.000]	0.999 [0.998, 0.999]	0.998 [0.996, 0.998]
Difference entropy	1.000 [1.000, 1.000]	0.999 [0.999, 0.999]	0.997 [0.995, 0.998]
Sum average	0.999 [0.999, 1.000]	0.999 [0.999, 0.999]	0.997 [0.995, 0.998]
Sum variance	1.000 [1.000, 1.000]	0.999 [0.999, 1.000]	0.996 [0.994, 0.998]
Sum entropy	1.000 [1.000, 1.000]	0.999 [0.999, 1.000]	0.996 [0.993, 0.997]
Angular second moment	1.000 [1.000, 1.000]	1.000 [1.000, 1.000]	0.995 [0.992, 0.997]
Contrast	1.000 [1.000, 1.000]	0.999 [0.999, 1.000]	0.997 [0.996, 0.998]
Dissimilarity	1.000 [1.000, 1.000]	0.999 [0.999, 0.999]	0.996 [0.995, 0.998]
Inverse difference	1.000 [1.000, 1.000]	0.999 [0.999, 1.000]	0.998 [0.996, 0.998]
Normalized inverse difference	0.999 [0.998, 0.999]	0.975 [0.963, 0.984]	0.996 [0.994, 0.998]
Inverse difference moment	1.000 [1.000, 1.000]	0.999 [0.999, 1.000]	0.998 [0.996, 0.999]
Normalized inverse difference moment	0.997 [0.995, 0.998]	0.969 [0.955, 0.981]	0.994 [0.991, 0.996]
Inverse variance	1.000 [1.000, 1.000]	0.999 [0.999, 0.999]	0.994 [0.992, 0.997]
Correlation	1.000 [1.000, 1.000]	0.999 [0.999, 0.999]	0.995 [0.992, 0.997]
Autocorrelation	0.999 [0.999, 1.000]	0.999 [0.999, 0.999]	0.997 [0.995, 0.998]
Cluster tendency	1.000 [1.000, 1.000]	0.999 [0.999, 1.000]	0.996 [0.994, 0.998]
Cluster shade	1.000 [1.000, 1.000]	0.999 [0.999, 1.000]	0.996 [0.994, 0.997]
Cluster prominence	1.000 [1.000, 1.000]	0.999 [0.999, 1.000]	0.997 [0.995, 0.998]
Information correlation 1	1.000 [1.000, 1.000]	0.999 [0.999, 0.999]	0.997 [0.996, 0.998]
Information correlation 2	1.000 [1.000, 1.000]	0.999 [0.999, 1.000]	0.999 [0.998, 0.999]

Run length matrix features

Short runs emphasis	1.000 [1.000, 1.000]	0.999 [0.998, 0.999]	0.997 [0.996, 0.998]
Long runs emphasis	1.000 [1.000, 1.000]	0.999 [0.999, 1.000]	0.998 [0.998, 0.999]
Low grey level run emphasis	1.000 [1.000, 1.000]	0.999 [0.998, 0.999]	0.999 [0.998, 0.999]
High grey level run emphasis	0.999 [0.999, 1.000]	0.999 [0.999, 0.999]	0.996 [0.995, 0.998]
Short run low grey level emphasis	1.000 [1.000, 1.000]	0.998 [0.997, 0.999]	0.999 [0.998, 0.999]
Short run high grey level emphasis	1.000 [1.000, 1.000]	0.999 [0.999, 0.999]	0.997 [0.995, 0.998]
Long run low grey level emphasis	1.000 [1.000, 1.000]	0.999 [0.999, 0.999]	0.998 [0.997, 0.999]
Long run high grey level emphasis	1.000 [1.000, 1.000]	0.999 [0.999, 0.999]	0.994 [0.991, 0.996]
Grey level non-uniformity	1.000 [1.000, 1.000]	0.999 [0.999, 1.000]	0.999 [0.998, 0.999]
Normalized grey level non-uniformity	1.000 [1.000, 1.000]	0.999 [0.999, 1.000]	0.996 [0.993, 0.997]
Run length non-uniformity	1.000 [1.000, 1.000]	1.000 [1.000, 1.000]	0.993 [0.990, 0.996]
Normalized run length non-uniformity	1.000 [1.000, 1.000]	0.999 [0.998, 0.999]	0.998 [0.996, 0.998]
Run percentage	1.000 [1.000, 1.000]	0.999 [0.999, 1.000]	0.998 [0.997, 0.999]
Grey level variance	1.000 [1.000, 1.000]	0.999 [0.999, 1.000]	0.997 [0.995, 0.998]
Run length variance	1.000 [1.000, 1.000]	0.999 [0.999, 1.000]	0.999 [0.998, 0.999]
Run entropy	1.000 [1.000, 1.000]	0.999 [0.999, 1.000]	0.995 [0.992, 0.997]

Size zone matrix features

Small zone emphasis	0.998 [0.997, 0.999]	0.962 [0.944, 0.976]	0.979 [0.968, 0.987]
Large zone emphasis	0.999 [0.999, 1.000]	0.999 [0.998, 0.999]	0.986 [0.979, 0.991]
Low grey level emphasis	1.000 [1.000, 1.000]	0.992 [0.988, 0.995]	0.999 [0.998, 0.999]
High grey level emphasis	0.999 [0.999, 1.000]	0.999 [0.998, 0.999]	0.996 [0.993, 0.997]
Small zone low grey level emphasis	1.000 [1.000, 1.000]	0.977 [0.965, 0.985]	0.995 [0.992, 0.997]
Small zone high grey level emphasis	0.999 [0.999, 0.999]	0.995 [0.992, 0.997]	0.999 [0.998, 0.999]
Large zone low grey level emphasis	0.998 [0.997, 0.999]	0.999 [0.998, 0.999]	0.992 [0.988, 0.995]
Large zone high grey level emphasis	0.999 [0.998, 0.999]	0.998 [0.997, 0.999]	0.975 [0.963, 0.984]
Grey level non-uniformity	0.997 [0.996, 0.998]	0.998 [0.996, 0.999]	0.920 [0.882, 0.949]

Normalized grey level non-uniformity	0.999 [0.999, 0.999]	0.995 [0.993, 0.997]	0.994 [0.991, 0.996]
Zone size non-uniformity	0.998 [0.997, 0.999]	0.996 [0.995, 0.998]	0.944 [0.919, 0.964]
Normalized zone size non-uniformity	0.998 [0.997, 0.999]	0.971 [0.957, 0.982]	0.973 [0.959, 0.983]
Zone percentage	1.000 [1.000, 1.000]	0.998 [0.997, 0.999]	0.993 [0.989, 0.995]
Grey level variance	0.998 [0.998, 0.999]	0.998 [0.997, 0.999]	0.996 [0.993, 0.997]
Zone size variance	0.999 [0.999, 1.000]	0.999 [0.998, 0.999]	0.986 [0.979, 0.991]
Zone size entropy	0.998 [0.997, 0.999]	0.991 [0.986, 0.994]	0.938 [0.909, 0.960]

Distance zone matrix features

Small distance emphasis	1.000 [1.000, 1.000]	0.998 [0.997, 0.999]	0.994 [0.991, 0.996]
Large distance emphasis	1.000 [1.000, 1.000]	0.999 [0.999, 1.000]	0.999 [0.998, 0.999]
Low grey level emphasis	1.000 [1.000, 1.000]	0.996 [0.995, 0.998]	1.000 [1.000, 1.000]
High grey level emphasis	1.000 [1.000, 1.000]	0.999 [0.998, 0.999]	0.996 [0.993, 0.997]
Small distance low grey level emphasis	1.000 [1.000, 1.000]	0.996 [0.994, 0.997]	1.000 [1.000, 1.000]
Small distance high grey level emphasis	1.000 [0.999, 1.000]	0.999 [0.998, 0.999]	0.999 [0.998, 0.999]
Large distance low grey level emphasis	1.000 [1.000, 1.000]	0.998 [0.997, 0.999]	1.000 [0.999, 1.000]
Large distance high grey level emphasis	1.000 [1.000, 1.000]	0.999 [0.999, 1.000]	0.998 [0.997, 0.999]
Grey level non-uniformity	1.000 [1.000, 1.000]	1.000 [1.000, 1.000]	0.997 [0.996, 0.998]
Normalized grey level non-uniformity	1.000 [1.000, 1.000]	0.998 [0.998, 0.999]	0.995 [0.993, 0.997]
Zone distance non-uniformity	1.000 [1.000, 1.000]	0.998 [0.997, 0.999]	0.995 [0.993, 0.997]
Normalized zone distance non-uniformity	1.000 [1.000, 1.000]	0.998 [0.997, 0.999]	0.995 [0.992, 0.997]
Zone percentage	1.000 [1.000, 1.000]	0.999 [0.999, 1.000]	0.997 [0.995, 0.998]
Grey level variance	1.000 [1.000, 1.000]	0.999 [0.998, 0.999]	0.996 [0.994, 0.998]
Zone distance variance	1.000 [1.000, 1.000]	1.000 [1.000, 1.000]	0.999 [0.999, 0.999]
Zone distance entropy	1.000 [1.000, 1.000]	1.000 [0.999, 1.000]	0.992 [0.988, 0.995]

Neighborhood grey tone difference matrix features

Coarseness	1.000 [1.000, 1.000]	1.000 [1.000, 1.000]	0.997 [0.995, 0.998]
Contrast	0.999 [0.998, 0.999]	1.000 [1.000, 1.000]	0.999 [0.999, 0.999]
Busyness	0.999 [0.998, 0.999]	0.999 [0.998, 0.999]	1.000 [0.999, 1.000]
Complexity	0.998 [0.997, 0.999]	0.998 [0.998, 0.999]	0.997 [0.996, 0.998]
Strength	0.999 [0.998, 0.999]	0.999 [0.998, 0.999]	0.999 [0.998, 0.999]

Neighboring grey level dependence matrix features

Low dependence emphasis	1.000 [0.999, 1.000]	0.998 [0.997, 0.999]	0.993 [0.990, 0.996]
High dependence emphasis	1.000 [1.000, 1.000]	0.999 [0.998, 0.999]	0.999 [0.998, 0.999]
Low grey level count emphasis	0.993 [0.989, 0.995]	0.999 [0.999, 1.000]	0.982 [0.973, 0.989]
High grey level count emphasis	0.996 [0.994, 0.997]	0.999 [0.999, 0.999]	0.979 [0.969, 0.987]
Low dependence low grey level emphasis	1.000 [1.000, 1.000]	0.989 [0.984, 0.993]	0.990 [0.985, 0.994]
Low dependence high grey level emphasis	1.000 [1.000, 1.000]	0.999 [0.998, 0.999]	0.997 [0.995, 0.998]
High dependence low grey level emphasis	0.999 [0.999, 1.000]	0.999 [0.998, 0.999]	0.993 [0.990, 0.996]
High dependence high grey level emphasis	0.999 [0.999, 1.000]	0.997 [0.995, 0.998]	0.978 [0.967, 0.986]
Grey level non-uniformity	0.991 [0.986, 0.994]	0.999 [0.999, 1.000]	0.950 [0.927, 0.968]
Normalized grey level non-uniformity	0.998 [0.997, 0.999]	1.000 [0.999, 1.000]	0.971 [0.957, 0.981]
Dependence count non-uniformity	0.986 [0.979, 0.991]	0.999 [0.999, 1.000]	0.885 [0.836, 0.925]
Normalized dependence count non-uniformity	1.000 [1.000, 1.000]	0.998 [0.996, 0.998]	0.992 [0.988, 0.995]
Dependence count percentage	1.000 [1.000, 1.000]	1.000 [1.000, 1.000]	1.000 [1.000, 1.000]
Grey level variance	0.998 [0.997, 0.999]	0.999 [0.999, 1.000]	0.996 [0.994, 0.998]
Dependence count variance	1.000 [1.000, 1.000]	0.992 [0.988, 0.995]	0.994 [0.992, 0.996]
Dependence count entropy	0.997 [0.995, 0.998]	0.997 [0.996, 0.998]	0.964 [0.947, 0.977]
Dependence count energy	0.997 [0.995, 0.998]	0.997 [0.995, 0.998]	0.971 [0.957, 0.982]

Table N10: Reproducibility of standardized features on the validation cohort, organized by feature and modality. A two-way random effects, single rater, absolute agreement intraclass correlation coefficient (ICC) and its 95% confidence interval were used to assess reproducibility. *NA*: the feature was standardized but values were computed by less than two team; *NS*: the feature was not standardized.

Accepted version 2020-01-07

Supplementary note L: Causes of deviations

We identified several causes of deviations from the reference values for standardized features, including:

- The image interpolation grid required careful definition (see IBSI reference manual sections 2.4 and 5.2.1) to make radiomics features in phase II reproducible.
- Interpolation was sometimes conducted at half precision (16-bit), which led to deviations in interpolated intensities.
- The absence of mesh-based volume representation caused associated morphological features to deviate noticeably for smaller regions of interest, such as the digital phantom (see section 3.1 of the IBSI reference manual). This was mostly because surface area would be computed in different ways.
- Inconsistent use of distance units (e.g. cm instead of mm). This was an issue for morphological features that are not dimensionless.
- The indexation of the rows and columns in texture matrices needed to be consistent and include rows and columns that only contain zero-valued elements. For example, intensities 2 and 5 are missing in the digital phantom. Dropping associated rows or columns from a texture matrix is incorrect and caused deviations.
- In the early stages, names of contributed features were occasionally difficult to match to the same feature definition, which was also reported previously (17–19). We recommend using names and nomenclature presented in the IBSI reference manual.
- Prior to the definition of morphological and intensity ROI masks, intensity-based re-segmentation of the ROI mask would lead to deviations. Some teams attempted to close small holes prior to computing morphological features, whereas others would leave them as is.
- Intensity-histogram entropy was sometimes computed directly from the image intensities, without binning.
- Neighbourhood grey tone difference matrix based features busyness, complexity and strength were sometimes computed without excluding discretized grey level probabilities equal to zero.

References

1. Tustison NJ, Avants BB, Cook PA, et al. N4ITK: improved N3 bias correction. *IEEE Trans Med Imaging*. 2010;29(6):1310–1320.
2. Zwanenburg A, Leger S, Agolli L, et al. Assessing robustness of radiomic features by image perturbation. *Sci Rep*. 2019;9(1):614.
3. Zwanenburg A, Leger S, Starke S, Löck S. Medical Image Radiomics Processor. <https://github.com/oncoray/mirp>.
4. Vallières M, Freeman CR, Skamene SR, El Naqa I. A radiomics model from joint FDG-PET and MRI texture features for the prediction of lung metastases in soft-tissue sarcomas of the extremities. *Phys Med Biol*. 2015;60(14):5471–5496.
5. Vallières M, Kay-Rivest E, Perrin LJ, et al. Radiomics strategies for risk assessment of tumour failure in head-and-neck cancer. *Sci Rep*. 2017;7(1):10117.
6. Zhou H, Vallières M, Bai HX, et al. MRI features predict survival and molecular markers in diffuse lower-grade gliomas. *Neuro Oncol*. 2017;19(6):862–870.
7. Götz M, Nolden M, Maier-Hein K. MITK Phenotyping: An open-source toolchain for image-based personalized medicine with radiomics. *Radiother Oncol*. 2019;131:108–111.
8. van Griethuysen JJM, Fedorov A, Parmar C, et al. Computational Radiomics System to Decode the Radiographic Phenotype. *Cancer Res*. 2017;77(21):e104–e107.
9. Apte AP, Iyer A, Crispin-Ortuzar M, et al. Technical Note: Extension of CERR for computational radiomics: A comprehensive MATLAB platform for reproducible radiomics research. *Med Phys*. 2018;45(8):3713–3720.
10. Cid YD, Castelli J, Schaer R, et al. QuantImage: An online tool for high-throughput 3D radiomics feature extraction in PET-CT. *Biomedical Texture Analysis*. Elsevier; 2017. p. 349–377.
11. Echegaray S, Bakr S, Rubin DL, Napel S. Quantitative Image Feature Engine (QIFE): an Open-Source, Modular Engine for 3D Quantitative Feature Extraction from Volumetric Medical Images. *J Digit Imaging*. 2018;31(4):403–414.
12. Pfaehler E, Zwanenburg A, de Jong JR, Boellaard R. RaCaT: An open source and easy to use radiomics calculator tool. *PLoS One*. 2019;14(2):e0212223.
13. Rathore S, Bakas S, Pati S, et al. Brain Cancer Imaging Phenomics Toolkit (brain-CaPTk): An Interactive Platform for Quantitative Analysis of Glioblastoma. In: Crimi A, Bakas S, Kuijf H, Menze B, Reyes M, editors. *Brainlesion: Glioma, Multiple Sclerosis, Stroke and Traumatic Brain Injuries*. Cham: Springer International Publishing; 2018. p. 133–145.
14. Davatzikos C, Rathore S, Bakas S, et al. Cancer imaging phenomics toolkit: quantitative imaging analytics for precision diagnostics and predictive modeling of clinical outcome. *J Med Imaging*. 2018;5(1):011018.
15. Nioche C, Orlhac F, Boughdad S, et al. LIFEx: A Freeware for Radiomic Feature Calculation in Multimodality Imaging to Accelerate Advances in the Characterization of Tumor Heterogeneity. *Cancer Res*. 2018;78(16):4786–4789.
16. Ashrafinia S. Quantitative nuclear medicine imaging using advanced image reconstruction and radiomics. Johns Hopkins University; 2019.
17. Buvat I, Orlhac F, Soussan M. Tumor Texture Analysis in PET: Where Do We Stand? *J. Nucl. Med*. 2015. p. 1642–1644.

1
2
3
4
5
6
7
8
9
10
11
12
13
14
15
16
17
18
19
20
21
22
23
24
25
26
27
28
29
30
31
32
33
34
35
36
37
38
39
40
41
42
43
44
45
46
47
48
49
50
51
52
53
54
55
56
57
58
59
60

18. Hatt M, Tixier F, Pierce L, Kinahan PE, Le Rest CC, Visvikis D. Characterization of PET/CT images using texture analysis: the past, the present... any future? Eur J Nucl Med Mol Imaging. 2017;44(1):151–165.

19. Foy JJ, Robinson KR, Li H, Giger ML, Al-Hallaq H, Armato SG. Variation in algorithm implementation across radiomics software. J Med Imaging. 2018;5(4):044505.

Accepted version 2020-01-07

IBSI guidelines for reporting on radiomics studies

Checklist - Version 1.0 (October 2019)

This checklist focuses specifically on in-depth reporting of studies involving radiomics. Other reporting guidelines may be applicable as well, e.g. STROBE (observational studies), CONSORT (randomised trials).

Not all items may be applicable. Indicate only applicable items.

Topic	Item	Description	Page
Patient			
Region of interest ¹	1	Describe the region of interest that is being imaged.	
Patient preparation	2a	Describe specific instructions given to patients prior to image acquisition, e.g. fasting prior to imaging.	
	2b	Describe administration of drugs to the patient prior to image acquisition, e.g. muscle relaxants.	
	2c	Describe the use of specific equipment for patient comfort during scanning, e.g. ear plugs.	
Radioactive tracer	PET, SPECT	3a	Describe which radioactive tracer was administered to the patient, e.g. 18F-FDG.
	PET, SPECT	3b	Describe the administration method.
	PET, SPECT	3c	Describe the injected activity of the radioactive tracer at administration.
	PET, SPECT	3d	Describe the uptake time prior to image acquisition.
	PET, SPECT	3e	Describe how competing substance levels were controlled. ²
Contrast agent		4a	Describe which contrast agent was administered to the patient.
		4b	Describe the administration method.
		4c	Describe the injected quantity of contrast agent.
		4d	Describe the uptake time prior to image acquisition.
		4e	Describe how competing substance levels were controlled.
Comorbidities	5	Describe if the patients have comorbidities that affect imaging. ³	
Acquisition⁴			
Acquisition protocol	6	Describe whether a standard imaging protocol was used, and where its description may be found.	
Scanner type	7	Describe the scanner type(s) and vendor(s) used in the study.	
Imaging modality	8	Clearly state the imaging modality that was used in the study, e.g. CT, MRI.	
Static/dynamic scans	9a	State if the scans were static or dynamic.	

¹ Also referred to as volume of interest.

² An example is glucose present in the blood which competes with the uptake of 18F-FDG tracer in tumour tissue. To reduce competition with the tracer, patients are usually asked to fast for several hours and a blood glucose measurement may be conducted prior to tracer administration.

³ An example of a comorbidity that may affect image quality in 18F-FDG PET scans are type I and type II diabetes melitus, as well as kidney failure.

⁴ Many acquisition parameters may be extracted from DICOM header meta-data, or calculated from them.

		Dynamic scans	9b	Describe the acquisition time per time frame.
		Dynamic scans	9c	Describe any temporal modelling technique that was used.
Scanner calibration			10	Describe how and when the scanner was calibrated.
Patient instructions			11	Describe specific instructions given to the patient during acquisition, e.g. breath holding.
Anatomical motion correction			12	Describe the method used to minimise the effect of anatomical motion.
Scan duration			13	Describe the duration of the complete scan or the time per bed position.
Tube voltage	CT		14	Describe the peak kilo voltage output of the X-ray source.
Tube current	CT		15	Describe the tube current in mA.
Time-of-flight	PET		16	State if scanner time-of-flight capabilities are used during acquisition.
RF coil	MRI		17	Describe what kind RF coil used for acquisition, incl. vendor.
Scanning sequence	MRI		18a	Describe which scanning sequence was acquired.
	MRI		18b	Describe which sequence variant was acquired.
	MRI		18c	Describe which scan options apply to the current sequence, e.g. flow compensation, cardiac gating.
Repetition time	MRI		19	Describe the time in ms between subsequent pulse sequences.
Echo time	MRI		20	Describe the echo time in ms.
Echo train length	MRI		21	Describe the number of lines in k-space that are acquired per excitation pulse.
Inversion time	MRI		22	Describe the time in ms between the middle of the inverting RF pulse to the middle of the excitation pulse.
Flip angle	MRI		23	Describe the flip angle produced by the RF pulses.
Acquisition type	MRI		24	Describe the acquisition type of the MRI scan, e.g. 3D.
k-space traversal	MRI		25	Describe the acquisition trajectory of the k-space.
Number of averages/ excitations	MRI		26	Describe the number of times each point in k-space is sampled.
Magnetic field strength	MRI		27	Describe the nominal strength of the MR magnetic field.
Reconstruction⁵				
In-plane resolution			28	Describe the distance between pixels, or alternatively the field of view and matrix size.
Image slice thickness			29	Describe the slice thickness.
Image slice spacing			30	Describe the distance between image slices. ⁶
Convolution kernel	CT		31a	Describe the convolution kernel used to reconstruct the image.
	CT		31b	Describe settings pertaining to iterative reconstruction algorithms.
Exposure	CT		31c	Describe the exposure (in mAs) in slices containing the region of interest.
Reconstruction method	PET		32a	Describe which reconstruction method was used, e.g. 3D OSEM.
	PET		32b	Describe the number of iterations for iterative reconstruction.
	PET		32c	Describe the number of subsets for iterative reconstruction.
Point spread function modelling	PET		33	Describe if and how point-spread function modelling was performed.
Image corrections	PET		34a	Describe if and how attenuation correction was performed.
	PET		34b	Describe if and how other forms of correction were performed, e.g. scatter correction, randoms correction, dead time correction etc.

⁵ Many reconstruction parameters may be extracted from DICOM header meta-data.

⁶ Spacing between image slicing is commonly, but not necessarily, the same as the slice thickness.

Reconstruction method	MRI	35a	Describe the reconstruction method used to reconstruct the image from the k-space information.
	MRI	35b	Describe any artifact suppression methods used during reconstruction to suppress artifacts due to undersampling of k-space.
Diffusion-weighted imaging	DWI-MRI	36	Describe the b-values used for diffusion-weighting.

Image registration

Registration method		37	Describe the method used to register multi-modality imaging.
---------------------	--	----	--

Image processing - data conversion

SUV normalisation	PET	38	Describe which standardised uptake value (SUV) normalisation method is used.
ADC computation	DWI-MRI	39	Describe how apparent diffusion coefficient (ADC) values were calculated.
Other data conversions		40	Describe any other conversions that are performed to generate e.g. perfusion maps.

Image processing - post-acquisition processing

Anti-aliasing		41	Describe the method used to deal with anti-aliasing when down-sampling during interpolation.
Noise suppression		42	Describe methods used to suppress image noise.
Post-reconstruction smoothing filter	PET	43	Describe the width of the Gaussian filter (FWHM) to spatially smooth intensities.
Skull stripping	MRI (brain)	44	Describe method used to perform skull stripping.
Non-uniformity correction ⁷	MRI	45	Describe the method and settings used to perform non-uniformity correction.
Intensity normalisation		46	Describe the method and settings used to normalise intensity distributions within a patient or patient cohort.
Other post-acquisition processing methods		47	Describe any other methods that were used to process the image and are not mentioned separately in this list.

Segmentation

Segmentation method		48a	Describe how regions of interest were segmented, e.g. manually.
		48b	Describe the number of experts, their expertise and consensus strategies for manual delineation.
		48c	Describe methods and settings used for semi-automatic and fully automatic segmentation.
		48d	Describe which image was used to define segmentation in case of multi-modality imaging.
Conversion to mask		49	Describe the method used to convert polygonal or mesh-based segmentations to a voxel-based mask.

Image processing - image interpolation

Interpolation method		50a	Describe which interpolation algorithm was used to interpolate the image.
		50b	Describe how the position of the interpolation grid was defined, e.g. align by center.
		50c	Describe how the dimensions of the interpolation grid were defined, e.g. rounded to nearest integer.
		50d	Describe how extrapolation beyond the original image was handled.
Voxel dimensions		51	Describe the size of the interpolated voxels.
Intensity rounding	CT	52	Describe how fractional Hounsfield Units are rounded to integer values after interpolation.

Image processing - ROI interpolation

⁷ Also known as bias-field correction.

Interpolation method	53	Describe which interpolation algorithm was used to interpolate the region of interest mask.
Partially masked voxels	54	Describe how partially masked voxels after interpolation are handled.
Image processing - re-segmentation		
Re-segmentation methods	55	Describe which methods and settings are used to re-segment the ROI intensity mask.
Image processing - discretisation		
Discretisation method ⁸	56a	Describe the method used to discretise image intensities.
	56b	Describe the number of bins (FBN) or the bin size (FBS) used for discretisation.
	56c	Describe the lowest intensity in the first bin for FBS discretisation. ⁹
Image processing - image transformation		
Image filter ¹⁰	57	Describe the methods and settings used to filter images, e.g. Laplacian-of-Gaussian.
Radiomics feature computation		
Feature set	58	Describe which set of radiomics features is computed and refer to their definitions or provide these.
IBSI compliance	59	State if the software used to extract the set of features is able to reproduce the IBSI feature reference values. ¹¹
Robustness	60	Describe how robustness of the features was assessed, e.g. test-retest analysis.
Software availability	61	Describe which software and version was used to compute features.
Radiomics feature computation - texture parameters		
Texture matrix aggregation	62	Define how texture-matrix based features were computed from underlying texture matrices.
Distance weighting	63	Define how CM, RLM, NGTDM and NGLDM weight distances, e.g. no weighting.
CM symmetry	64	Define whether symmetric or asymmetric co-occurrence matrices were computed.
CM distance	65	Define the (Chebyshev) distance at which co-occurrence of intensities is determined, e.g. 1.
SZM linkage distance	66	Define the distance and distance norm for which voxels with the same intensity are considered to belong to the same zone for the purpose of constructing an SZM, e.g. Chebyshev distance of 1.
DZM linkage distance	67	Define the distance and distance norm for which voxels with the same intensity are considered to belong to the same zone for the purpose of constructing a DZM, e.g. Chebyshev distance of 1.
DZM zone distance norm	68	Define the distance norm for determining the distance of zones to the border of the ROI, e.g. Manhattan distance.
NGTDM distance	69	Define the neighbourhood distance and distance norm for the NGTDM, e.g. Chebyshev distance of 1.
NGLDM distance	70	Define the neighbourhood distance and distance norm for the NGLDM, e.g. Chebyshev distance of 1.
NGLDM coarseness	71	Define the coarseness parameter for the NGLDM, e.g. 0.

⁸ Discretisation may be performed separately to create intensity-volume histograms. If this is indeed the case, this should be described as well.

⁹ This is typically set by range re-segmentation.

¹⁰ The IBSI has not introduced image transformation into the standardised image processing scheme, and is in the process of benchmarking various common filters. This section may therefore be expanded in the future.

¹¹ A software is compliant if and only if it is able to reproduce the feature reference values for the digital phantom and for one or more image processing configurations using the radiomics CT phantom. Reviewers may demand that you provide the IBSI compliance spreadsheet for your software.

Machine learning and radiomics analysis

Diagnostic and prognostic modelling	72	See the TRIPOD guidelines for reporting on diagnostic and prognostic modelling.
Comparison with known factors	73	Describe where performance of radiomics models is compared with known (clinical) factors.
Multicollinearity	74	Describe where the multicollinearity between radiomics features in the signature is assessed.
Model availability	75	Describe where radiomics models with the necessary pre-processing information may be found.
Data availability	76	Describe where imaging data and relevant meta-data used in the study may be found.

The reporting guidelines presented above are a copy of the guidelines found in section 4.1 of the IBSI reference manual (see online supplemental materials).